Check for updates

Received: 23 June 2023 | Revised: 27 August 2023 | Accepted: 31 August 2023

DOI: 10.1002/cey2.500

REVIEW

CARBON ENERGY WILEY

Metal halide perovskites for solar-to-chemical energy conversion in aqueous media

Chunhua Wang[1] | **Yang Ding**[2] | **Yannan Wang**[3] | **Zhirun Xie**[1] | **Zhiyuan Zeng**[4] | **Xin Li**[5] | **Yun Hau Ng**[1]

[1]School of Energy and Environment, Low-Carbon and Climate Impact Research Centre, City University of Hong Kong, Hong Kong SAR, China

[2]Center of Advanced Optoelectronic Materials, College of Materials and Environmental Engineering, Hangzhou Dianzi University, Hangzhou, China

[3]Department of Materials Engineering, KU Leuven, Leuven, Belgium

[4]Department of Materials Science and Engineering, and State Key Laboratory of Marine Pollution, City University of Hong Kong, Hong Kong SAR, China

[5]Key Laboratory of Energy Plants Resource and Utilization, Ministry of Agriculture and Rural Affairs, Institute of Biomass Engineering, South China Agricultural University, Guangzhou, China

Correspondence
Chunhua Wang and Yun Hau Ng, School of Energy and Environment, Low-Carbon and Climate Impact Research Centre, City University of Hong Kong, 83 Tat Chee Ave, Kowloon, Hong Kong SAR, China.
Email: chunhua.wang@cityu.edu.hk and yunhau.ng@cityu.edu.hk

Funding information
City University of Hong Kong, Grant/Award Number: SIRG 7020022; Hong Kong Research Grant Council (RGC), Grant/Award Numbers: GRF CityU 11305419, GRF CityU 11306920, GRF CityU 11308721, GRF CityU 11316522

Abstract

Solar-driven energy conversion is a promising technology for a sustainable energy future and environmental remediation, and an efficient catalyst is a key factor. Recently, metal halide perovskites (MHPs) have emerged as promising photocatalysts due to their exceptional photoelectronic properties and low-cost solution processing, enabling successful applications in H_2 evolution, CO_2 reduction, organic synthesis, and pollutant degradation. Despite these successes, the practical applications of MHPs are limited by their water instability. In this review, the recently developed strategies driving MHP-catalyzed reactions in aqueous media are outlined. We first articulate the structures and properties of MHPs, followed by elaborating on the origin of instability in MHPs. Then, we highlight the advances in solar-driven MHP-based catalytic systems in aqueous solutions, focusing on developing external protection strategies and intrinsically water-stable MHP materials. With each approach offering peculiar sets of advantages and challenges, we conclude by outlining potentially promising opportunities and directions for MHP-based photocatalysis research in aqueous conditions moving forward. We anticipate that this timely review will provide some inspiration for the design of MHP-based photocatalysts, manifestly stimulating their applications in aqueous environments for solar-to-chemical energy conversion.

KEYWORDS
aqueous media, metal halide perovskites, photocatalysis, stability, water

This is an open access article under the terms of the Creative Commons Attribution License, which permits use, distribution and reproduction in any medium, provided the original work is properly cited.
© 2024 The Authors. *Carbon Energy* published by Wenzhou University and John Wiley & Sons Australia, Ltd.

1 | INTRODUCTION

Modern civilization is facing an increasing need to exploit green energy sources to reduce the reliance on fossil fuels and alleviate environmental pollution. Of the many available alternatives, solar energy is by far the most abundant and easily accessible.[1,2] Since the pioneering work reported by Fujishima and Honda,[3] converting solar energy to chemical fuels through semiconductor-based photocatalysis promises a green and sustainable energy economy. To date, several reaction systems, including powder suspension, thin film photocatalyst, and photoelectrode, have been developed.[4–6] Especially, the design of heterojunctions (Schottky, type-II, and Z-scheme) has enabled improvement in photocatalytic performance.[7] Although the configurations vary, the key factor determining the photoactivity is the semiconductor photocatalyst. Thus, the quest for novel photocatalysts to drive photoredox reactions with robust performance continues.

Over the past decade, metal halide perovskites (MHPs) have triggered interdisciplinary interest and revolutionized optoelectronic fields due to their fantastic properties, such as broad light absorption range, high charge mobility, long carrier diffusion length, and low-cost solution processing.[8–10] So far, thanks to the much effort made by people from all backgrounds, MHPs have set multiple records in solar cells, light-emitting diodes, and photodetectors. Inspired by these successes, the utilization of MHPs for solar-to-chemical energy conversion through photocatalytic processes has also gained much attention in recent years.[11–13] Especially, MHPs endow tunable bandgap, multiple exciton generation, defect tolerance, and facile preparation characteristics.[14] Additionally, the morphology and size of MHP nanostructures can be readily controlled using different synthesis technologies such as hot injection, ligand-assisted reprecipitation, and mechanochemical treatment.[15] These features make MHPs highly suitable as photocatalysts for various photoredox systems and thus have recently sparked significant interest in photocatalysis.

Since the first work reported by Park et al. in 2016 who used $CH_3NH_3PbI_3$ ($MAPbI_3$) as the photocatalyst for H_2 generation,[16] MHPs have been successfully adopted for photocatalytic H_2 evolution, CO_2 reduction, organic synthesis, and pollutant degradation (Figure 1A), and the flourish of the research was witnessed by the number of publications (Figure 1B). Despite the encouraging achievements, MHPs generally have low formation enthalpies originating from the softness of crystal-chemical bonds, making them easy to form while also degrading under internal stimuli (humidity, heat, O_2, UV irradiation, etc.).[4,17,18] Especially due to the ionic nature, MHPs are readily decomposed to a PbX_2 precipitate, a $MA^+/FA^+/Cs^+$ cation, and a halide anion when exposed to water/polar solvents. Undoubtedly, the stability issue has been considered the main bottleneck that limits their further applications. This could be the reason why MHP photovoltaics (PVs) have everlastingly flourished since 2009, while MHP photocatalysis did not emerge until December 2016. So far, although tremendous efforts have

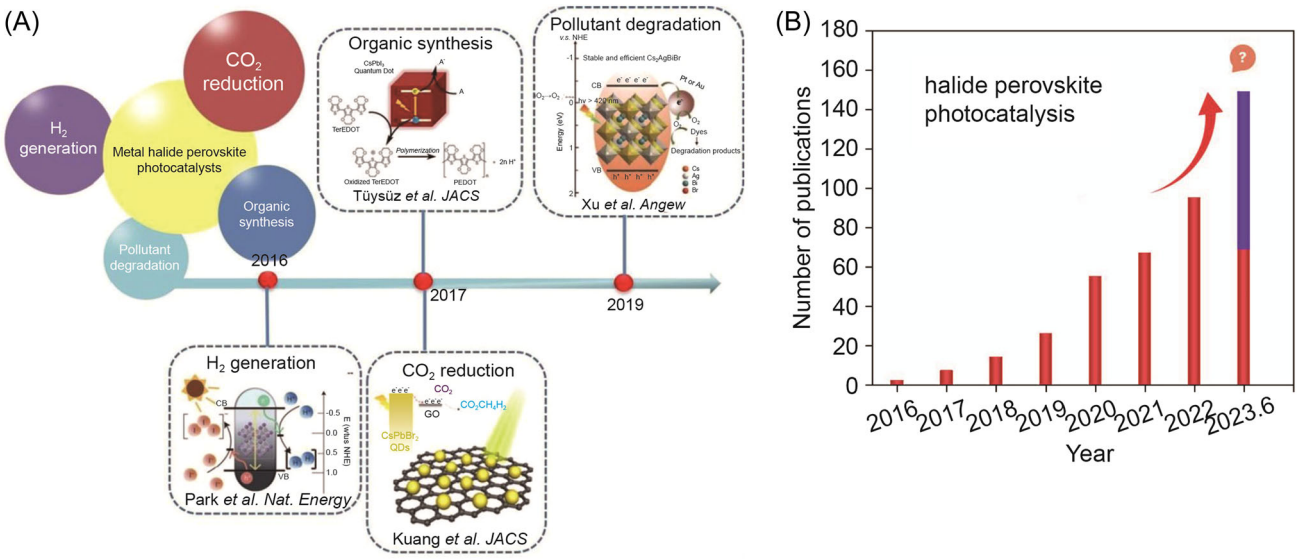


FIGURE 1 (A) Timeline showing the MHP-based photocatalysis systems in H_2 evolution, CO_2 reduction, organic synthesis, and pollutant degradation applications. Reproduced with permission: Copyright 2020, Elsevier.[13] (B) The number of publications on MHP-based photocatalysis obtained from Scopus database. MHP, metal halide perovskite.

26379368, 2024, 11, Downloaded from https://onlinelibrary.wiley.com/doi/10.1002/cey2.500, Wiley Online Library on [04/09/2026]. See the Terms and Conditions (https://onlinelibrary.wiley.com/terms-and-conditions) on Wiley Online Library for rules of use; OA articles are governed by the applicable Creative Commons License

been made regarding MHP photocatalytic applications, most reactions are still performed in low-polarity organic solvents, while conducting in aqueous environments is still challenging.[17] To improve the stability of MHPs in aqueous media, some strategies have been recently developed, ranging from physical protection (such as core-shell structure) to composition engineering of MHP material. Based on these studies, some recent reviews have pointed out the stability issue of MHP photocatalysts.[4,7,13,15] For example, Wang et al.[15] discussed how to rationally design the MHP nanocrystals for photocatalytic CO_2 reduction; Pan et al.[4] summarized the MHP materials for photo(electro)chemical applications. Teo et al.[7] clarified the challenges of MHPs for sustainable energy development and environmental remediation. However, a systematic report on the advancements of photocatalytic solar-to-chemical energy conversion in aqueous media, especially the promises and challenges, is still lacking, while it is of crucial importance for moving the MHP-based photocatalysis forward.

In this review, we outlined the advances and challenges of MHP-based photocatalysis in aqueous media. First, we gave a brief introduction to MHPs, elaborating on the structure, optical and electronic properties, and the advantages of MHPs when applied to photocatalysis. Second, we highlighted the water instability property of MHPs when in contact with water or other polar solvents, disclosing a critical analysis of both organic–inorganic hybrids and all-inorganic MHPs by a combination of experimental and theoretical results. Following this, we put emphasis on the recently developed strategies allowing for MHP photocatalytic reactions carried out in aqueous solutions, including extrinsic physical protection and intrinsic composition engineering. Finally, we cast a personal perspective on the future challenges and possibilities toward targeting MHP photocatalysis in real-world aqueous environments. This review is anticipated to inspire researchers to design MHP-stabilized photocatalytic systems for efficient photocatalytic reactions.

2 | BASICS OF MHPs

MHPs, a novel group of sophisticated materials used in various light-based technologies, have piqued a high interest from academia and industry due to their easy synthesis as well as extraordinary optical and electrical properties.[4,7,15] More specifically, the excellent optical properties include high light absorption (absorption coefficient $> 10^{-5}\,cm^{-1}$), low exciton binding energy ($E_b < k_bT$ in the triiodide family), tunable bandgap (1.2–3.6 eV), and so on; meanwhile the fantastic electrical properties contain high carrier mobility ($\sim 10^2\,cm^2\,V^{-1}\,s^{-1}$), large diffusion length (~1 μm), long charge carrier lifetime (~1 μs), and so on. MHPs have galvanized the solar cell community after the pioneering work reported by Kojima et al.[19] Besides solar cells, MHPs have also been employed for light-emitting diodes (LEDs), photodetectors, X-ray detectors, lasers, luminescent solar concentrators, and photocatalysis.[20–24] In this section, the basic information of MHPs will be clarified.

2.1 | Fundamental structure

Before discussing the MHPs, we briefly review the very relevant perovskite oxides, which are a group of materials with a similar crystal structure of $CaTiO_3$—the earliest perovskite material brought to light by Gustav Rose 1839 while named after Russian mineralogist Lev Perovski.[20] The crystal structure of perovskite oxides consists of a three-dimensional (3D) network of corner-sharing $[TiO_6]^{8-}$ octahedra with a 12-fold coordinated Ca^{2+} cation occupying the interstice formed by eight surrounding octahedrons. The above crystal structure for MHPs is generally expressed as the chemical formula ABX_3.[20,25] In this formula, A site can be a monovalent organic cation such as MA^+ ($CH_3NH_3^+$), FA^+ ($CH(NH_2)_2^+$), PEA^+ ($C_8H_{12}N^+$), DMA^+ ($C_2H_8N^+$), and so on, or an inorganic cation like Cs^+, K^+, Rb^+, and so on; B site is a bivalent metal cation (e.g., Pb^{2+}, Sn^{2+}, Ge^{2+}, Sb^{2+}, Eu^{2+}, etc.) and X is a halide anion (e.g., I^-, Br^-, and Cl^-). Typically, A occupies a corner of a unit cell, B sites in a body-centered position, and X occupies a face-centered position, with a corner-sharing $[BX_6]^{4-}$ octahedra,[26] as exhibited in Figure 2A.

The structure of MHPs is associated with $[BX_6]^{4-}$ octahedra and A cation, and element radii play a critical part in the structure. Their crystal structures can be tuned by regulating its octahedral factor (μ) (Equation 1) and long-standing Goldschmidt's tolerance factor τ (Equation 2)[28]:

$$\mu = \frac{r_B}{r_X}, \tag{1}$$

$$\tau = \mu^{-1} - n_A\left[n_A - \frac{\frac{r_A}{r_B}}{\ln\left(\frac{r_A}{r_B}\right)}\right], \tag{2}$$

where r_A, r_B, and r_X are the radii of A, B, and X ions, respectively, and n_A is the varied oxidation state of A. For all-inorganic MHPs involving alkali A^+ cations, $n_A = 1$.

26379368, 2024, 11, Downloaded from https://onlinelibrary.wiley.com/doi/10.1002/cey2.500, Wiley Online Library on [04/09/2026]. See the Terms and Conditions (https://onlinelibrary.wiley.com/terms-and-conditions) on Wiley Online Library for rules of use; OA articles are governed by the applicable Creative Commons License

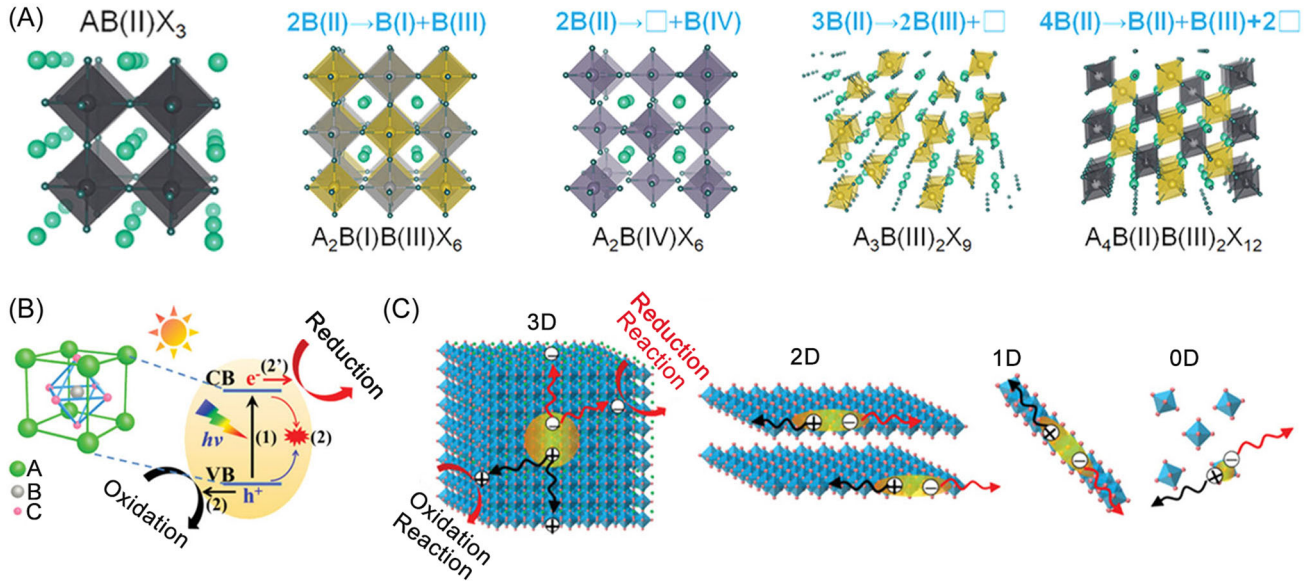


FIGURE 2 (A) The crystal structure of ABX_3 and its evolution to other representative alternatives. Reproduced with permission: Copyright 2022, Wiley-VCH.[27] (B) Schematic illustrating the photocatalytic reactions over MHP-based materials and (C) the reaction mechanisms with various dimensionalities ranging from 3D to 0D ([B and C] Reproduced with permission: Copyright 2021, Wiley-VCH[4]).

MHPs contain three different crystal structures: cubic phase (α), tetragonal phase (β), and orthorhombic phase (γ).[28] Typically, τ is used to assess the degrees of size matching between the A cation and BX_6 octahedra. An ideal high-symmetry cubic structure can be achieved at $0.9 < \tau < 1.0$ in which $\tau = 1.0$ indicates a perfect fit of an A site cation within the BX_3 framework, whereas octahedral deformity and loss in symmetry are predicted when $\tau < 1.0$, resulting in a less symmetric tetragonal or orthorhombic structure in the range of $0.81 < \tau < 0.9$.[29] Beyond the upper limit of the τ factor, nonperovskite is formed due to lattice distortion, and low-dimensional derivatives can be generated when τ exceeds this range. When $\tau > 1.0$, a NH_4CdI_3-type crystal structure is usually favored.[29] When $\tau < 0.8$, a $CsNiBr_3$-type crystal structure is most likely to form. Consequently, stable 3D MHP crystals can be formed when $0.81 < \tau < 1.0$ and $0.44 < \mu < 0.90$.

Cation types and valence states can cause changes in the radii of the MHPs, leading to lattice deformation and crystal phase changeover.[30] The tilting process relieves the mismatch between the shrinking A-X framework and the rigid $[BX_6]^{4-}$ octahedron. At a higher tolerance factor of greater than 1.0, an oversize A-site cation is likely beyond its fitting range, while the A-site cation is too small to fit in the cavities when $\tau < 0.8$, thus leading to the formation of nonperovskite structures. Note that the size of the A cation, in particular, affects the symmetry of MHPs structure, causing distortions in the B-X bonds and thus changing the electrical properties of the MHPs. Therefore, A site ion greatly links to the photocatalytic rate during the photocatalytic processes.[7] By contrast, B and X elements are mainly responsible for constructing energy levels,[27] which determine the photocatalytic performance to a large extent since the photoredox ability highly relies on the oxidation (valence band [VB]) and reduction (conduction band [CB]) potentials.[31] Here the clarification can be subdivided into organic-inorganic hybrid and all-inorganic MHPs. For instance, in terms of the former one, the organic A cation does not govern the band structure, but its size is a critical matter that judges the formability of the MHP structure, where a larger cation results in an expansion of the MHP lattice while a smaller one gives rise to the contraction of the lattice.[32] Among them, MA- and FA-based MHPs are the most used light-absorbing materials in solar cells owing to MA^+ and FA^+ cations with an ionic radius of 2.70 and 2.79 Å, respectively,[33] perfectly fit to the MHPs, allowing for less packing symmetry and higher efficiency than other cations. Moving to all-inorganic MHPs, Cs-based compounds have been explored widely, in which the Cs^+ with a radius of 1.81 Å[10,33] matches well the structure requirements of MHPs.

In addition to ABX_3 structure like $CsPbBr_3$, other derivatives (Figure 2A) such as $A_2B(I)B(III)X_6$ ($Cs_2AgBiBr_6$, $Cs_2AgBiCl_6$), $A_2B(IV)X_6$ (Cs_2PbBr_6, Cs_2PbI_6, Cs_2SnCl_6), $A_3B_2X_9$ ($Cs_3Bi_2I_9$, $Cs_3Bi_2Br_9$, $Cs_3Sb_2I_9$, $Rb_3Sb_2I_9$), and $A_4B(II)B(III)_2X_{12}$ ($Cs_4MnBi_2Cl_{12}$, $Cs_4CdSb_2Cl_{12}$, $Cs_4CdBi_2Cl_{12}$) have also been reported.[27] Note that there are some differences between these derivatives and the typical ABX_3 structures. $A_2B(I)B(III)X_6$ MHPs are generally called double perovskites since their vacancy-ordered structures[17]; $A_2B(IV)X_6$ MHPs have a similar

26379368, 2024, 11, Downloaded from https://onlinelibrary.wiley.com/doi/10.1002/cey2.500, Wiley Online Library on [04/09/2026]. See the Terms and Conditions (https://onlinelibrary.wiley.com/terms-and-conditions) on Wiley Online Library for rules of use; OA articles are governed by the applicable Creative Commons License

name to double perovskites, but they have not gained much attention compared to $A_2B(I)B(III)X_6$. By contrast, $A_3B_2X_9$ as a type of typical two-dimensional (2D) MHPs has been widely studied.[13] $A_4B(II)B(III)_2X_{12}$ MHPs, however, do not have the perovskite structures like the typical ABX_3, and there is still limited research on them.[27] Beyond this range, an oversized A-cation triggers the formation of lower-dimensional layered or confined perovskites instead of a three-dimensional (3D) MHP structure. So far, some oversized organic cations such as dimethylammonium (DMA^+, $CH_3NH_2CH_3^+$), ethylammonium (EA^+, $CH_3CH_2NH_3^+$), guanidinium (GA^+, $C(NH_2)_3^+$), and acetamidinium (AA^+, $CH_3C(NH_2)_2^+$) have been reported.[18] By contrast, a strained lattice would form if the A-cation is too small.

On the basis of the spatial configurations, that is, connectivity of corner-sharing $[BX_6]^{4-}$ octahedra, four types of dimensionalities of MHPs can be obtained (Figure 2B): 3D, 2D, one-dimensional (1D), and zero-dimensional (0D) because of either different level of corner-sharing between $[BX_6]^{4-}$ octahedral anions or different crystal shapes. Besides the bulk 3D MHPs, 0D (quantum dots), 1D (nanowires, nanorods), and 2D (nanosheets) have been widely explored to date. Such a dimensionality change from 3D to low-dimensional structures leads to different optical and electronic properties like bandgap and density of states (DOS), thus showing the great potential in photocatalytic applications.

2.2 | Properties of MHPs

MHPs have fantastic physical and chemical properties due to their unique proportions and constituent elements. All in all, the excellent optoelectronic performance of MHP materials is mainly attributed to their distinctive electronic structures. Through investigation of the electronic structure such as band structure and DOS, their photoelectric properties, including light absorption coefficient, exciton binding energy (E_b), effective mass, charge mobility, and charge recombination rate, can be analyzed.

Theoretical simulations such as density functional theory (DFT) have been widely employed so far. Calculation results indicate that the electronic structures of MHPs with different halides possess similar features.[34] For instance, in typical 3D all-inorganic $CsPbX_3$ (X = I, Br, and Cl), the VB of the MHPs is constituted by the antibonding hybridized 6s orbitals of Pb and X np orbitals of the halides ($n = 5$, 4, and 3 for I, Br, and Cl, respectively), and the CB is mainly composed of Pb 6p orbitals.[34,35] The band structures are rarely dependent on X composition, while X ions affect the bandgap (E_g). The excitation and charge carrier recombination are mainly confined within the $[PbX_6]^{4-}$ octahedra. Furthermore, more photoelectronic parameters can also be obtained. Compared with traditional semiconductor materials, MHPs possess excellent optical properties, including high absorption coefficient ($>10^5\ cm^{-1}$), small exciton binding energy ($E_b < k_bT$ for iodide-based family), and tunable bandgap (1.24–3.55 eV).[36]

One of the major advantages MHPs possess is that their optical bandgap can be tuned over the visible light region. Normally, the A cation does not affect the position of the CB and VB as described above and thus has a minor contribution to the E_g. Regarding Pb-based organic and inorganic hybrid MHPs, the E_g changes with increasing tilting angle of Pb-X-Pb and distorted lattices.[18] Here, we will focus on the case of inorganic MHPs. Taking $CsPbX_3$ MHP as an example, the halide composition can be effective in tuning E_g. When changing X site halide from I to Br and Cl, the energy levels of the X (np) orbitals decrease, shifting the CB position toward more positive potentials,[34] thus yielding different E_g. Specifically, $CsPbI_3$ with cubic phase has an E_g of 1.73 eV; a wider E_g was found for $CsPbBr_3$ (2.3 eV) and $CsPbCl_3$ (2.99 eV). Besides, the E_g is tunable by mixing different halides. For example, $CsPbI_xBr_{3-x}$ samples like $CsPbI_2Br$ and $CsPbIBr_2$ have an E_g of 1.92 and 2.05 eV, respectively.[37] Meanwhile, E_g is also found to be affected by the final stoichiometry in the case of ions of comparable size and shape. The advancements in tailoring low-dimension MHPs also lead to increased bandgap energy due to the quantum confinement effect.[38] For MHP quantum dots and nanowires, their diameters were also seen to affect the bandgap energy. Overall, the ease of composition engineering makes a wide controllable E_g for MHPs (Figure 3B), which meets well the photocatalysis requirements. In this case, MHPs in principle almost suit various photoredox applications.

The stability of materials is also a key factor in evaluating their practical applications. For MHPs, it has been indicated that they generally suffer from stability issues under light irradiation in the presence of O_2, especially the I-based compounds, which originates from the introduction of oxygen in the lattice of MHPs with the creation of iodide vacancies upon photoexcitation.[40,41] With the photogenerated electrons, these oxygen molecules would form reactive superoxide species ($^{\bullet}O_2^-$), which react with organic cations, thus leading to the decomposition of MHPs. Through UV-visible absorption spectroscopy (UV-vis) and X-ray diffraction (XRD) characterizations, Ito et al.[42] reported that $CH_3NH_3PbI_3$ decomposes into PbI_2 under light exposure for 12 h. The degradation mechanism was further investigated by Aristidou et al.[40] They showed that this photoinduced

26379368, 2024, 11, Downloaded from https://onlinelibrary.wiley.com/doi/10.1002/cey2.500, Wiley Online Library on [04/09/2026]. See the Terms and Conditions (https://onlinelibrary.wiley.com/terms-and-conditions) on Wiley Online Library for rules of use; OA articles are governed by the applicable Creative Commons License

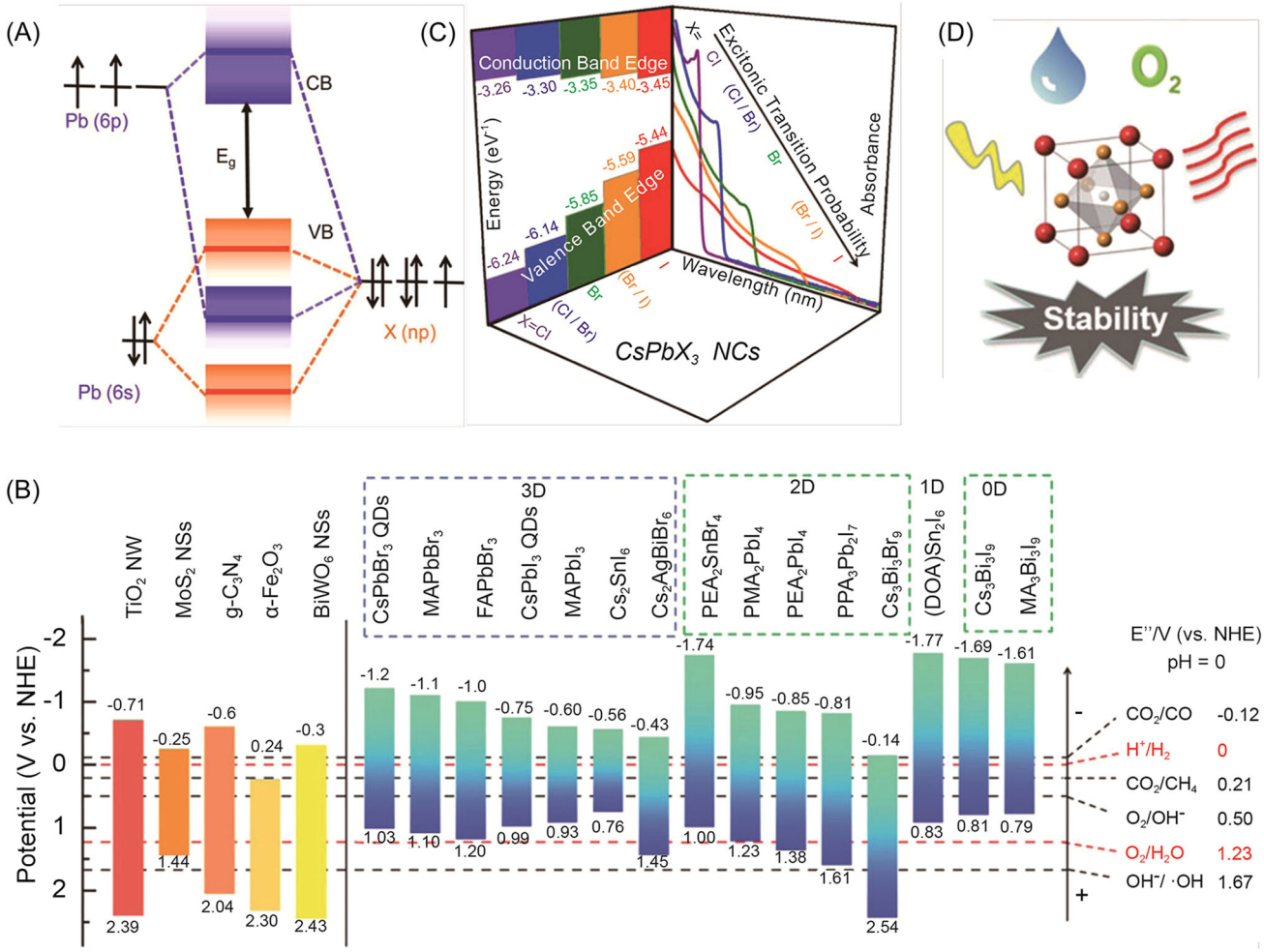


FIGURE 3 (A) Schematic illustration of bonding/antibonding orbitals of $APbX_3$ showing the layout of the VB and CB. Reproduced with permission: Copyright 2016, American Chemical Society.[34] (B) A comparison of the band energy levels of MHPs with some traditional semiconductors. Reproduced with permission: Copyright 2021, Wiley-VCH.[4] (C) Tunable bandgap/absorption of $CsPbX_3$ with halide composition engineering. Reproduced with permission: Copyright 2016, American Chemical Society.[34] (D) Schemes of the stability issue of MHPs regarding moisture and O_2 under light irradiation. Reproduced with permission: Copyright 2018, Wiley-VCH.[39] CB, conduction band; MHP, metal halide perovskite; VB, valence band.

degradation process is associated with iodide vacancies, in which O_2 will be inserted into the crystal lattice of MHPs. The molecular O_2 will react with photogenerated electrons at the site of iodide vacancies to form reactive superoxide species. Then, the superoxide radicals interact with MA and produce the decomposed products, including H_2O, CH_3NH_2, PbI_2, and I_2. This was thought to be mitigated by the introduction of inorganic cations (such as Cs), which generally render more chemical and photostability in polar solvents. However, even if the stability can be improved to a certain extent, the oxygen reaching the grain boundary still can degrade the MHPs.[17] Note that halide defects are also essential factors in MHP photostability. While halide vacancies can produce contact polarization improving charge transfer, halide abundance provides the routes to oxygen present in MHPs lattice.[43]

The last one that needs to be mentioned is water stability, which is the most notorious characteristic of MHPs since MHPs tend to degrade quickly when in contact with water molecules due to the ionic nature; thus, this greatly limits their practical photocatalytic applications. This review will focus on highlighting the effect of water on MHP-based photocatalysis, with the degradation mechanisms presented in Section 3, which is followed by elaborating on the recently developed strategies that enable the conduct of MHP photocatalytic reactions in aqueous media.

2.3 | Importance of MHPs

Since the end of 2016, MHPs have been developed as promising materials for photocatalytic applications. Until

26379368, 2024, 11, Downloaded from https://onlinelibrary.wiley.com/doi/10.1002/cey2.500, Wiley Online Library on [04/09/2026]. See the Terms and Conditions (https://onlinelibrary.wiley.com/terms-and-conditions) on Wiley Online Library for rules of use; OA articles are governed by the applicable Creative Commons License

now, MHPs have gained popularity in various photocatalytic application fields due to their distinct optoelectronic properties. Generally, a photoredox reaction is mainly determined by three processes[44,45]: (1) light absorption of the photocatalysts to produce photogenerated electron-hole pairs, (2) charge separation and migration to reactive sites of the photocatalysts surface, and (3) photoredox reactions' occurrence on the surface of the photocatalysts. Based on this criterion, some of the key points that support the superior photocatalytic performance of the MHPs include[46–48]: (i) easily tunable E_g (1.2–3.6 eV) and high optical absorption coefficient ($>10^{-5}\,cm^{-1}$), (ii) long carrier diffusion length (~1 μm) and relatively low charge recombination rate (carrier lifetime can reach up to a few μs), and (iii) well-balanced charge transfers (carrier mobility: $\sim 10^2\,cm^2\,V^{-1}\,s^{-1}$) suitable for redox reactions.

To be specific, first, the redox potential of photogenerated charge carriers can be manipulated in a large range via composition engineering of MHPs, which makes most of the photocatalytic processes thermodynamically feasible. Second, the band structures and charge migration properties of MHPs can easily be altered through chemical composition tuning and morphology engineering. Third, the ferroelectric and piezoelectric effects of MHPs may further contribute to photoactivity.[49] Fourth, as clarified above, for most of MHPs, their dimensionality and particle size control can be easily manipulated; therefore, a roadmap can look toward fabricating 2D, 1D, and 0D MHPs with desirable size range, which can provide abundant active sites for photoredox reactions or/and offer a large surface to load cocatalysts. Finally, unlike conventional photocatalysts that normally suffer complicated preparation and expensive precursors, MHPs can be easy to fabricate through low-cost solution processing. These aforementioned superior properties over the traditional photocatalysts make the MHPs more attractive. Another important point that needs to be mentioned is that although MHP-based photocatalytic applications started from Pb-contained compounds ($MAPbI_3$, $CsPbBr_3$, etc.) in the beginning, nowadays many alternatives such as tin (Sn^{2+}), bismuth (Bi^{3+}), and antimony (Sb^{3+}) are exploited to avoid the use of toxic Pb, with some representatives like $CsSnBr_3$, $Cs_3Bi_2Br_9$ and $Cs_3Sb_2Br_9$ or cation pairs like silver (Ag^+) and bismuth (Bi^{3+})/indium (In^{3+}) forming double MHPs ($Cs_2AgBiBr_6$, $Cs_2AgInCl_6$), enabling the MHP materials to be environmentally friendly semiconductors.[17]

From the viewpoint of photocatalysis, achieving high photocatalytic performance is always the goal. Along with the photoactivity race, a notorious process being emphasized frequently is the fast charge recombination of the photocatalysts. For MHP nanocrystals, their defect tolerance property offers the leverage to endow high charge carrier utilization efficiency,[17] thus contributing to high photocatalytic efficiency. In addition, due to the easily tunable composition and a large number of compounds, the band structure, electronic structure, adsorption properties, and size of MHP materials can be

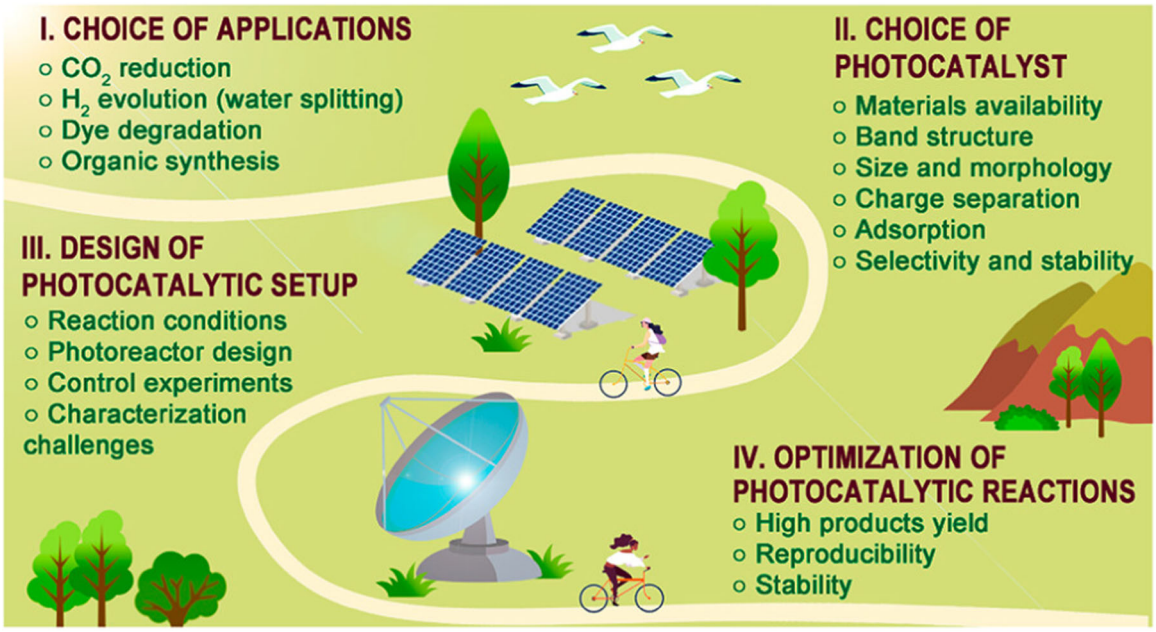


FIGURE 4 Detailed research directions on MHP-based photocatalysis. Reproduced with permission: Copyright 2022, American Chemical Society.[50] MHP, metal halide perovskite.

26379368, 2024, 11, Downloaded from https://onlinelibrary.wiley.com/doi/10.1002/cey2.500, Wiley Online Library on [04/09/2026]. See the Terms and Conditions (https://onlinelibrary.wiley.com/terms-and-conditions) on Wiley Online Library for rules of use; OA articles are governed by the applicable Creative Commons License

tweaked through accurate design to improve the photoactivity and the selectivity of products. Overall, these excellent properties of MHPs make them promising materials for driving effective photocatalytic reactions. Based on the current status, Figure 4 summarizes the promising opportunities and directions for moving MHP-based photocatalysis research forward. In this review, we mainly focus on the stability issue (part IV), that is, the promise and challenges of MHPs-based photocatalysts in aqueous solutions.

3 | DEGRADATION MECHANISMS IN WATER MEDIA

The fantastic optoelectronic properties of MHPs have attracted much attention in photocatalytic applications in recent years. However, the main drawback that hinders their further development is the stability issue, especially their instability against water since most MHPs are very sensitive to water and tend to be degraded rapidly when in contact with water molecules due to the soft nature of MHPs materials.[17,43] This section will clarify and highlight the mechanisms of the degradation behaviors.

Generally, MHPs show the chemical formula of ABX_3, where the three components A (MA^+, FA^+, Cs^+), B (Pb^{2+}, Sn^{2+}), and X (I^-, Br^-, Cl^-) are either weakly bonded by ionic interactions (e.g., for Pb-I bonds, the bonding energy is about 142 kJ mol^{-1}) and/or secondary bonds such as van der Waals interactions.[17] Additionally, MHPs normally exhibit low formation enthalpies due to the softness of crystal-chemical bonds (e.g., the theoretical decomposition energy barriers of about 0.1 eV for $MAPbI_3$).[51,52] Therefore, MHPs can be easily formed and are also easily damaged, which is particularly serious for the self-assembly crystallized organic-inorganic hybrid MHPs and limits their further applications. Figure 5A schematically illustrates the degradation processes of the MHPs as a function of the molar ratio of water to MHPs.[53] Note that the degradation behaviors of MHPs are highly related to the water quantity; that is, the structural breakdown is on a grade-by-grade basis (vide infra). That is the reason why a deliberate addition of trace amounts of water to the precursor solution or the exposure of the prepared MHP thin films in controlled humidity environments has been shown to improve the crystallinity and optical properties of MHPs and thus improve the solar cells/LEDs

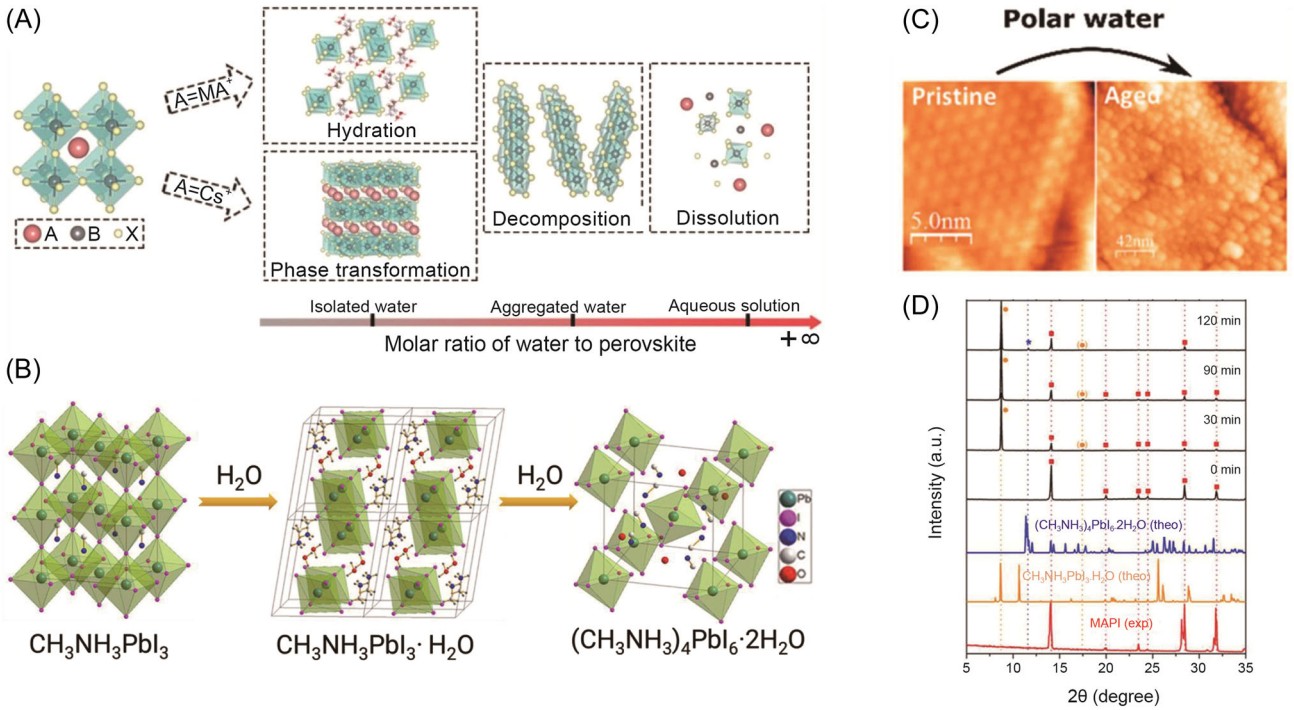


FIGURE 5 (A) Schematic illustration of the interactions between MHPs and water. Reproduced with permission: Copyright 2022, American Chemical Society.[53] (B) Structural transformation of $CH_3NH_3PbI_3$, with the intermediates monohydrate $CH_3NH_3PbI_3{\cdot}H_2O$ and dihydrate $(CH_3NH_3)_4PbI_6{\cdot}2H_2O$. Reproduced with permission: Copyright 2015, American Chemical Society.[54] (C) Scanning tunneling microscopy images of MHP single crystal surface before and after exposure to water. Reproduced with permission: Copyright 2016, American Chemical Society.[55] (D) Time-resolved XRD patterns showing the hydration of $CH_3NH_3PbI_3$ thin films. Reproduced with permission: Copyright 2015, American Chemical Society.[54] MHP, metal halide perovskite.

26379368, 2024, 11, Downloaded from https://onlinelibrary.wiley.com/doi/10.1002/cey2.500, Wiley Online Library on [04/09/2026]. See the Terms and Conditions (https://onlinelibrary.wiley.com/terms-and-conditions) on Wiley Online Library for rules of use; OA articles are governed by the applicable Creative Commons License

conversion efficiencies. While this is not the focus of this paper, interested readers are encouraged to explore the cited literature.[56–59] In our case, the reaction media are the aqueous solutions that far exceed the degradation threshold (0.003 mM mL^{-1} in solvent) of the MHPs.[60] To describe the stability of the MHPs clearly, two categorized groups, that is, organic-inorganic hybrid MHPs (such as $MAPbI_3$ and $FAPbI_3$) and inorganic MHPs ($CsPbBr_3$, $Cs_2AgBiBr_6$, etc.), will be discussed separately.

Hybrid MHPs with organic components at the A site, such as MA and FA, possess high chemical reactivity induced by polar surroundings of C–N or N–H bonding, which adverse the decomposition rate of the MHPs at polar surroundings such as in the presence of H_2O.[17] For instance, MA/FA-based MHPs are prone to degrade into PbX_2 components, MA or FA, and halide ions in contact with water due to the fragile organic moieties.[50] As a result, water cannot be used as a solvent in photocatalysis. Over the past decade, more efforts have been devoted to exploring the degradation mechanisms of MHPs, with advanced techniques such as in situ grazing incidence XRD and transient absorption spectroscopy techniques and ab initio molecular dynamics simulations.[61–63] These investigations showed that the absorbed H_2O quickly penetrates the inner structure of MHPs and reacts with BX_6 octahedra, resulting in the formation of monohydrate and dihydrate compounds at the beginning and ultimately decomposition to lose the crystalline structure and optoelectronic properties. Taking $CH_3NH_3PbI_3$ as an example, it tends to hydrate by first forming an intermediate monohydrate $CH_3NH_3PbI_3{\cdot}H_2O$ when exposed to H_2O and then dihydrate to $(CH_3NH_3)_4PbI_6{\cdot}2H_2O$ (Figure 5B),[54] which blocks carriers transport and instigate severe charge recombination. Scanning tunneling microscopy showed the obvious change in the morphology of MHP after exposure to water (Figure 5C).[55] Besides, in situ XRD further monitored the structural decomposition with a hydration process (Figure 5D).[54] The degradation processes can be explained by the following equations[56,61–63]:

$$CH_3NH_3PbI_3 + H_2O \rightarrow CH_3NH_3PbI_3{\cdot}H_2O, \quad (3)$$

$$4CH_3NH_3PbI_3 + 2H_2O \rightarrow (CH_3NH_3)_4PbI_6{\cdot}2H_2O + 3PbI_2, \quad (4)$$

$$CH_3NH_3PbI_3{\cdot}H_2O \rightarrow PbI_2 + CH_3NH_3I + H_2O, \quad (5)$$

$$CH_3NH_3I \rightarrow CH_3NH_2 + HI. \quad (6)$$

The instability issues of MHP photocatalysts have recently been highlighted by Huang et al. in a review.[64] Overall, it originates from their crystal structures. Owing to the ionic nature of MHPs, they generally have a "soft" structure. This causes the fast degradation of MHPs under photocatalytic conditions. To improve the stability of MHP materials, more studies have focused on finding alternatives to replace the MA or FA. Among them, Cs has been shown to be a promising candidate since it has inorganic properties and similar ionic radius relative to MA and FA,[33] with some prototypical compounds such as 0D Cs_4PbBr_6, 2D $CsPb_2Br_5$, and 3D $CsPbBr_3$. For instance, Cs_4PbBr_6, a representative 0D MHP, showed a high photoluminescence quantum yield (PLQY) and thus promising in both optoelectronics and photocatalysis applications.[65] Also, $CsPbBr_3$ has been widely used for various photocatalytic reactions due to its tunable morphologies. However, there is always a phase transition between these materials under trances of water (Figure 6A).[66] In fact, the ternary phase diagram (Figure 6B) of Cs, Pb, and Br indicates that Cs_4PbBr_6, $CsPb_2Br_5$, and $CsPbBr_3$ lie on the same segment whose endpoints are $PbBr_2$ and CsBr.[67] And they will be fully degraded into $PbBr_2$ and CsBr once the water is too much (vide infra). DFT calculation was employed to better understand the degradation behavior. Taking the most widely used $CsPbBr_3$ photocatalyst as an example, with the participation of H_2O, the potential barriers (ΔEp) required for $CsPbBr_3$ to $CsPb_2Br_5$ process is only 0.03 eV (Figure 6C),[68] indicating the easy decomposition features of MHPs. Experimental results further confirmed water treatment of the green-emitting phase having an intense Photoluminescence (PL) signal at 500 nm results in the transformation into another phase that has no optical activity (Figure 6D).[69] Raman mode of $CsPbBr_3$ at 72 cm^{-1} is significantly decreased and has almost disappeared (Figure 6E).[69] Moreover, some novel modes, apparently stemming from the precursors $PbBr_2$ and CsBr, emerge at 38 and 130 cm^{-1}. Therefore, as confirmed by the vibrational spectrum, the complete degradation of $CsPbBr_3$ from the green-emitting phase occurs by turning the material into its constituents, which is collaborated by the XRD results (Figure 6F).[69] Based on both experimental and theoretical investigations, their decomposition processes follow the below equations[66,69]:

$$Cs_4PbBr_6 \rightarrow CsPbBr_3 + 3CsBr, \quad (7)$$

$$2CsPbBr_3 \rightarrow CsPb_2Br_5 + CsBr, \quad (8)$$

$$CsPb_2Br_5 \rightarrow 2PbBr_2 + CsBr. \quad (9)$$

On the other hand, the existence of Pb in Cs-Pb-Br MHPs restricts their mass applications since Pb can

26379368, 2024, 11, Downloaded from https://onlinelibrary.wiley.com/doi/10.1002/cey2.500, Wiley Online Library on [04/09/2026]. See the Terms and Conditions (https://onlinelibrary.wiley.com/terms-and-conditions) on Wiley Online Library for rules of use; OA articles are governed by the applicable Creative Commons License

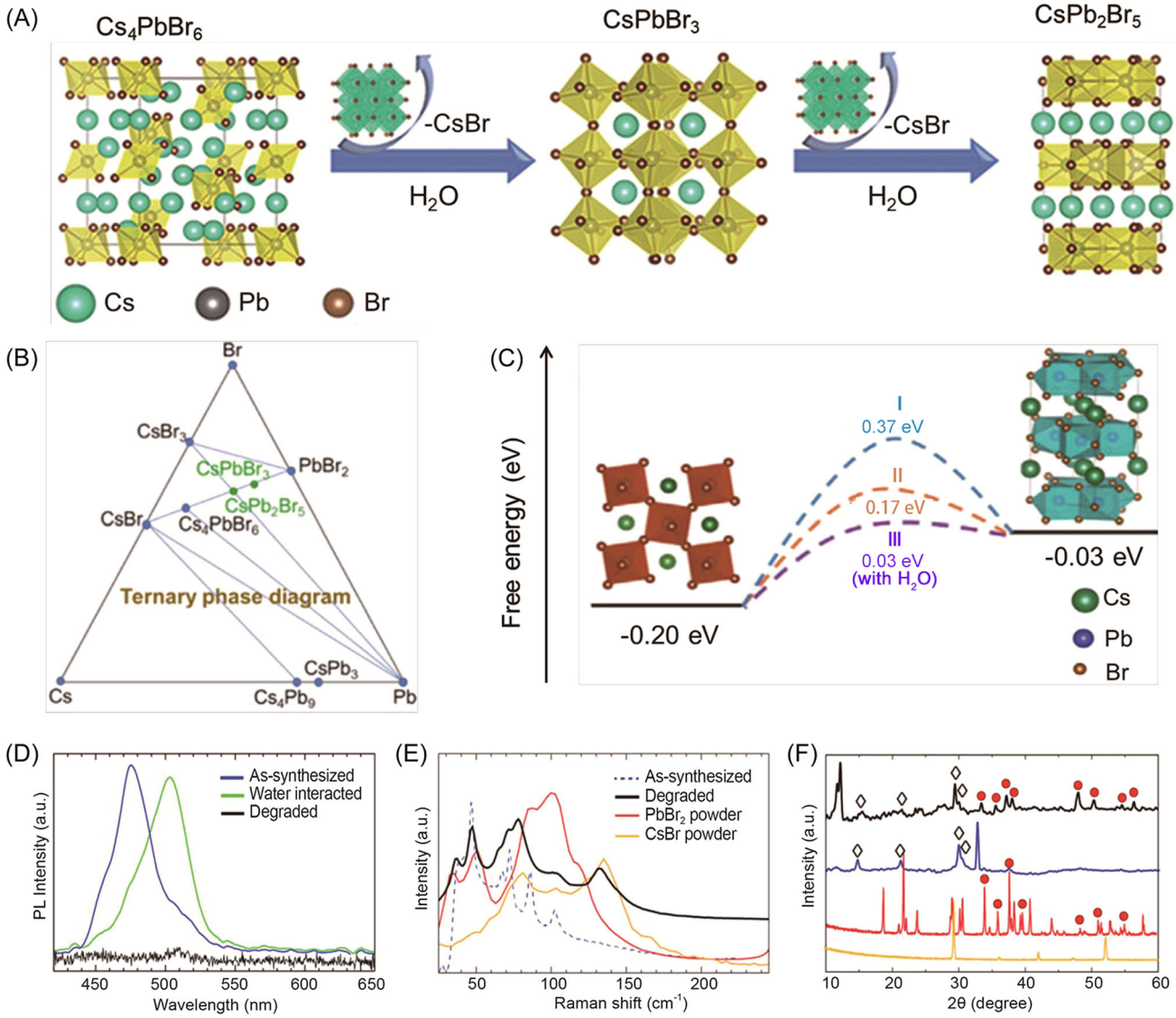


FIGURE 6 (A) Schematic illustration of the degradation of Cs_4PbBr_6, $CsPbBr_3$, and $CsPb_2Br_5$ in the presence of trace water. Reproduced with permission: Copyright 2021, Wiley-VCH.[66] (B) Ternary phase diagram of Cs, Pb, and Br, in which Cs_4PbBr_6, $CsPbBr_3$, and $CsPb_2Br_5$ lie between the precursors CsBr and $PbBr_2$ on the segment. Reproduced with permission: Copyright 2021, American Chemical Society.[67] (C) The potential barriers (ΔEp) need to be overcome for the interconversion from $CsPbBr_3$ to $CsPb_2Br_5$. Reproduced with permission: Copyright 2021, Wiley-VCH.[68] (D) PL spectra of $CsPbBr_3$ and the degraded materials. (E) Raman spectra of $CsPbBr_3$, the degraded crystals, with CsBr and $PbBr_2$ powders as the reference. (F) XRD patterns of $CsPbBr_3$ materials before and after degradation ([D–F] Reproduced with permission: Copyright 2018, American Physical Society[69]).

disturb the neurological, cardiovascular, and hematopoietic systems.[50] Along with the remarkable development of energy conversion efficiency, developing environmentally benign Pb-free MHPs is urgent. One straightforward idea to solve the Pb toxicity issue involves replacing the Pb with Sn or Ge from the same group of the periodic table. However, Sn or Ge is readily to be oxidized due to the high-energy 5s and 4s orbitals,[70] thus leading to the corresponding MHPs exhibiting extreme sensitivity to the ambient atmosphere. More research showed that using Bi or Sb to replace Pb provides a more stable solution. For instance, $Cs_2AgBiBr_6$, as a benchmark Pb-free double perovskite, has emerged as a promising alternative to Pb-containing MHPs because of its high stability, nontoxicity, exceptional optoelectronic properties, and multifunctionality.[27,50] Indeed, $Cs_2AgBiBr_6$ is more stable in air environments compared to MA/FA-based MHPs, which shows negligible structural change after exposure to air for 30 days.[70] Although the exciting result is shown in this study, $Cs_2AgBiBr_6$ still cannot against water.[70,71]

26379368, 2024, 11, Downloaded from https://onlinelibrary.wiley.com/doi/10.1002/cey2.500, Wiley Online Library on [04/09/2026]. See the Terms and Conditions (https://onlinelibrary.wiley.com/terms-and-conditions) on Wiley Online Library for rules of use; OA articles are governed by the applicable Creative Commons License

$$2Cs_2AgBiBr_6 \rightarrow CsAgBr_2 + AgBr + Cs_3Bi_2Br_9. \quad (10)$$

$$Cs_3Bi_2Br_9 \rightarrow 2CsBr + 2BiBr_3. \quad (11)$$

All in all, these representative MHP compounds outlined above indicate that the long-term stability of MHPs during the photocatalytic process still needs to be addressed before the practical applications. Indeed, tackling the issue at its roots is essential thinking. Under this context, much effort has been devoted to exploring water-stable MHP materials. Until now, some low-dimensional MHPs compounds have been shown to be able to conduct a photocatalytic reaction in water-containing environments.[17,43] On the other hand, for these 3D MHPs that are unstable in water media, some strategies have also been developed to keep them stable during photocatalytic processes,[4,17] such as creating a dynamic equilibrium, protecting the MHPs by forming a core-shell structure, using functional layers to minimize the destroy of water, or encapsulating the MHPs within a photoelectrochemical (PEC) system. This will be highlighted in the following section.

4 | MHP STABILIZATION STRATEGIES IN AQUEOUS SOLUTIONS

The instability issues of MHPs have motivated the development of several approaches toward realizing stable photocatalytic environments (Figure 7), including (i) creating a dynamic equilibrium by placing MHPs in saturated haloacid solutions, (ii) developing useful physical protection strategies (including designing core-shell structure, crafting functional layers, and constructing encapsulation layers via PEC systems) to screen the MHPs from water molecules, and (iii) exploring water-stable MHP materials. In this section, we will outline the current state of play for each of these approaches, highlighting their successes and challenges with specific examples along with the features which ultimately govern their realistic applications.

4.1 | Precipitation–solubility dynamic equilibrium

As clarified before, the hydrolysis-induced decomposition of MHPs in aqueous media is the key source of their intrinsic instability. Considering the ionic nature of MHPs which are water-soluble compounds, utilizing

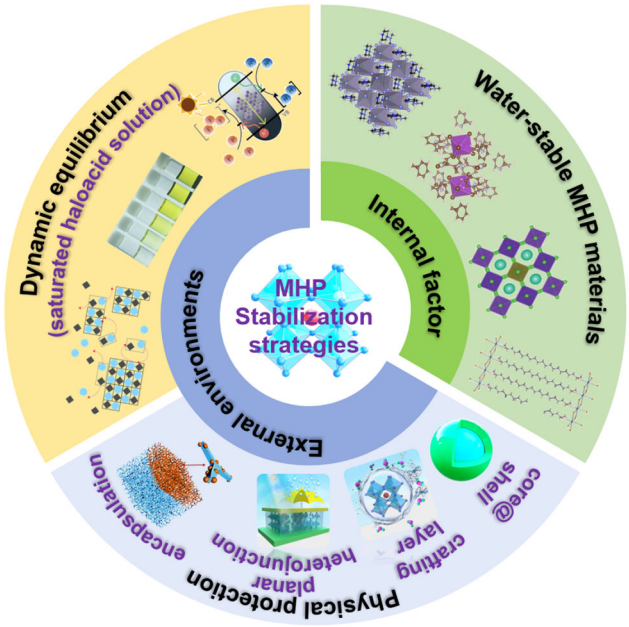


FIGURE 7 Summary of the currently developed stabilization strategies for MHPs that enable MHP-based photocatalysts for photoredox reactions in aqueous solutions. Reproduced with permission: Copyright 2016, Springer Nature.[16] Copyright 2021, Elsevier.[60] Copyright 2021, Wiley-VCH.[72] Copyright 2021, Wiley-VCH.[73] Copyright 2020, Wiley-VCH.[74] Copyright 2021, Wiley-VCH.[75] Copyright 2019, Wiley-VCH.[76] MHP, metal halide perovskite.

the precipitation–solubility equilibrium between the MHP phase and soluble ionic species (in a saturated haloacid solution) is a promising approach to address the stability issue.

In 2016, Nam et al. pioneered this innovative stabilization approach using $MAPbI_3$ as a photocatalyst in a saturated hydrogen iodide (HI) acid aqueous solution for photocatalytic H_2 generation.[16] Note that this is also the first work demonstrating that MHPs are promising materials for photocatalytic applications. Here, the $MAPbI_3$ first dissolves, forming MA^+ cations and PbI_3^- complex anions; meanwhile, an equal amount of $MAPbI_3$ phase will recrystallize, which is modulated by the I^- and H^+ ion concentrations (Figure 8A). A relatively high I^- concentration ($-\log[I^-] < -0.4$) is needed to guarantee the dissolution of PbI_3^-, and meanwhile, the acidity of the solution requires a certain level ($pH < -0.5$) to inhibit the formation of hydrates. The dynamic interfacial equilibrium of $MAPbI_3$/HI aqueous solution is shown in Figure 8B. To confirm the idea suitable for photocatalysis, photocatalytic HI splitting for H_2 evolution on $MAPbI_3$ was carried out. Under visible light irradiation ($\lambda \geq 475$ nm), an H_2 production rate of about 3 $\mu mol\ g^{-1}\ h^{-1}$ was achieved when using pure $MAPbI_3$ as the photocatalyst; during the catalytic process, the photogenerated electrons responsible for

26379368, 2024, 11, Downloaded from https://onlinelibrary.wiley.com/doi/10.1002/cey2.500, Wiley Online Library on [04/09/2026]. See the Terms and Conditions (https://onlinelibrary.wiley.com/terms-and-conditions) on Wiley Online Library for rules of use; OA articles are governed by the applicable Creative Commons License

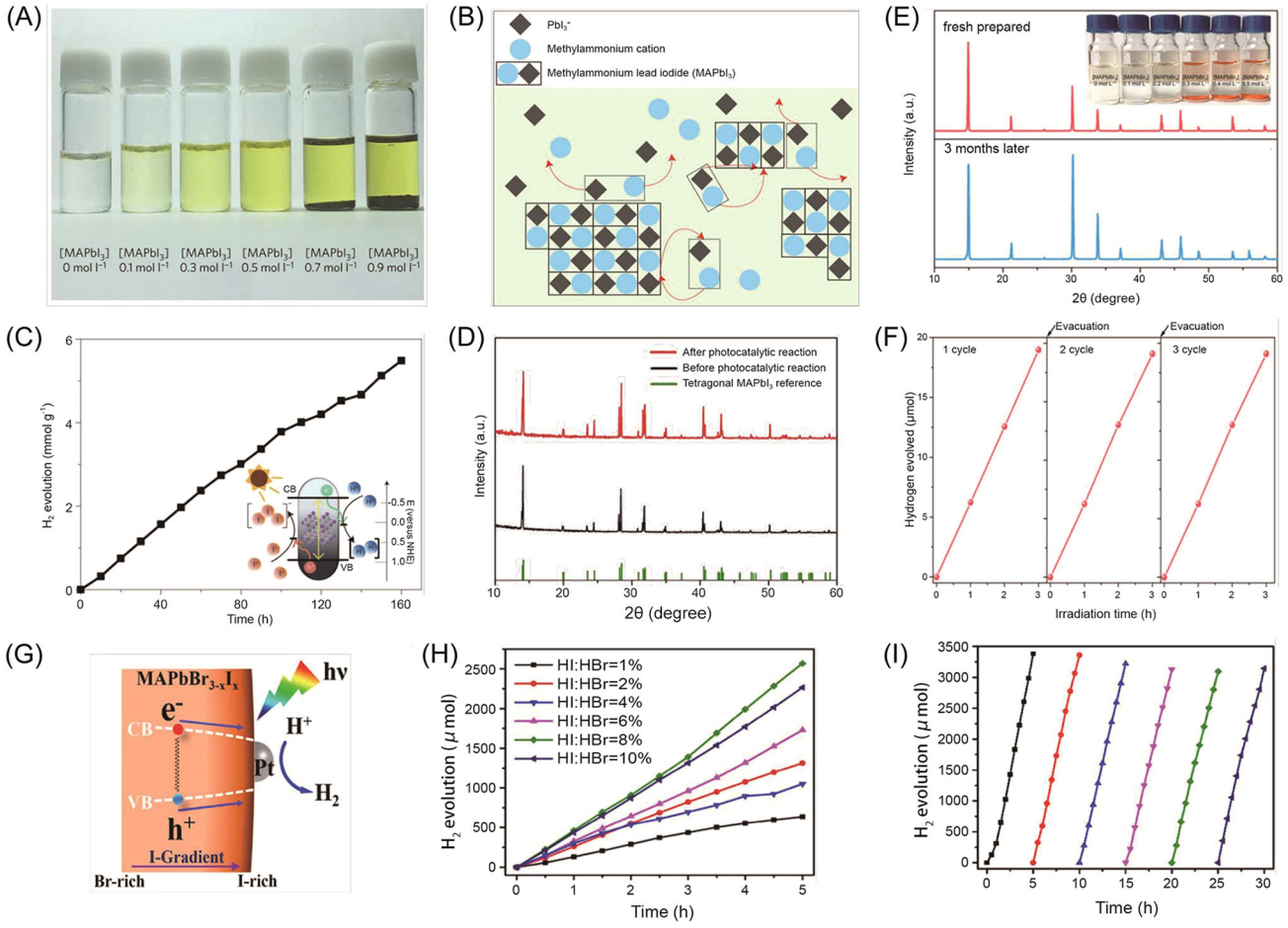


FIGURE 8 (A) Photographs of $MAPbI_3$ in aqueous HI solutions at various concentrations (0–0.9 mol L^{-1}). (B) Schematic illustrating the precipitation–solubility equilibrium, (C) stability test, and (D) XRD patterns of $MAPbI_3$ in HI aqueous solution for photocatalytic H_2 generation. Inset in Figure 8C shows the band diagram of $MAPbI_3$ for photocatalytic HI splitting ([A–D] Reproduced with permission: Copyright 2016, Springer Nature[16]). (E) XRD patterns of $MAPbBr_3$ immersed in aqueous HBr solution for 3 months. (F) Recycling test of $MAPbBr_3$ in HBr solution for H_2 production. Inset in Figure 8 E shows a picture of $MAPbBr_3$ powder in HI aqueous solution with a concentration from 0 to 0.5 mol L^{-1} ([E and F] Reproduced with permission: Copyright 2018, American Chemical Society[77]). (G) Scheme representing the photocatalytic H_2 production process, (H) the effect of HI/HBr ratio on the H_2 yield, and (I) stability tests over $MAPbBr_{3-x}I_x$ in an HBr/HI aqueous solution ([G–I] Reproduced with permission: Copyright 2018, American Chemical Society[78]).

generating H_2 molecules ($2H^+ + 2e^- \rightarrow H_2$) and holes driving the I^- to I_3^- oxidation ($3I^- + 2\,h^+ \rightarrow I_3^-$). Besides, to sustain the I^- concentration, H_3PO_2, a well-known good reducing agent for I_3^- to I^-, was added to the reaction system. Furthermore, the decoration of Pt on the $MAPbI_3$ surface enhanced the H_2 rate to roughly 57 μmol g^{-1} h^{-1}, yielding a solar-to-chemical conversion efficiency (solar HI splitting efficiency) of 0.81%. Impressively, $MAPbI_3$ maintained stable for 160 h during the cycling tests under continuous irradiation without compromise to the photoactivity (Figure 8C). XRD patterns (Figure 8D) further confirm that the $MAPbI_3$ phase was maintained. Following this work, many studies have been reported for photocatalytic H_2 generation over MHP-based composites in HI aqueous solutions, such as $MAPbI_3$/RGO,[79] $MAPbI_3$-Pt/TiO_2,[80] $MAPbI_3$/BP,[81] $MAPbI_3$/Ni_3C,[82] $MAPbI_3$/CoP,[83] $MAPbI_3$/MoS_2,[84] Cs_2SnI_6/Pt,[85] and $MA_3Bi_2I_9$/DMA_3BiI_6[86], with the target of improving the H_2 production rate. In addition to the champion photoactivity reaching ~13,600 μmol g^{-1} h^{-1} (Table 1), the measured time for the stability evaluation also exceeds 200 h, demonstrating the great potential of MHPs for photocatalytic H_2 evolution in the HI aqueous solution.

Although these encouraging results have been achieved, all the MHP photocatalysts used in these works are I-containing compounds since the I^- ion in HI aqueous solution is the key factor to maintaining the $MAPbI_3$ phase in a dynamic equilibrium fashion (Figure 8B). While the family of MHPs still includes a large number of Br- and Cl-based composites, can this method be extended to others? To answer this question, the solution is to put the Br-based MHP powder in HBr

26379368, 2024, 11, Downloaded from https://onlinelibrary.wiley.com/doi/10.1002/cey2.500, Wiley Online Library on [04/09/2026]. See the Terms and Conditions (https://onlinelibrary.wiley.com/terms-and-conditions) on Wiley Online Library for rules of use; OA articles are governed by the applicable Creative Commons License

TABLE 1 Summary of the developed strategies enabling solar-driven MHP catalytic reactions in aqueous media.

Strategy	Reaction types	Photocatalyst	Reaction medium	Light source	Activity	Stability	References
Dynamic equilibrium	H_2 generation	$MAPbI_3$-Pt/TiO_2	HI aqueous solution	Visible light ($\lambda \geq 420$ nm), 200 mW cm^{-2}	7300 μmol g^{-1} h^{-1}	12 h	[80]
		Cs_2SnI_6/Pt	HI aqueous solution	Visible light ($\lambda \geq 420$ nm), 300 W	430 μmol g^{-1} h^{-1}	24 h	[85]
		$MAPbI_3$/CoP	HI aqueous solution	Visible light ($\lambda \geq 420$ nm), 150 W	2087.5 μmol g^{-1} h^{-1}	27 h	[83]
		$MA_3Bi_2I_9$/DMA_3BiI_6	HI aqueous solution	Visible light ($\lambda \geq 420$ nm), 300 W	198.2 μmol g^{-1} h^{-1}	100 h	[86]
		$MAPbI_3$/Pt	HI aqueous solution	Visible light ($\lambda \geq 475$ nm)	57 μmol g^{-1} h^{-1}	160 h	[16]
		$MAPbI_3$/rGO	HI aqueous solution	Visible light ($\lambda \geq 420$ nm), 300 W	939 μmol g^{-1} h^{-1}	200 h	[79]
		$MAPbI_3$/BP	HI aqueous solution	Visible light ($\lambda \geq 420$ nm), 300 mW cm^{-2}	3472 μmol g^{-1} h^{-1}	200 h	[81]
		$MAPbI_3$/Ni_3C	HI aqueous solution	Visible light ($\lambda \geq 420$ nm), 300 W	2362 μmol g^{-1} h^{-1}	200 h	[82]
		$MAPbI_3$/MoS_2	HI aqueous solution	Visible light ($\lambda > 420$ nm), 300 W	13600 μmol g^{-1} h^{-1}	208 h	[84]
		PEDOT:PSS/ $MAPbBr_3$/Ta_2O_5	HBr aqueous solution	Visible light irradiation ($\lambda > 420$ nm), 150 mW cm^{-2}	650 μmol g^{-1} h^{-1}	4 h	[77]
		$CsPbBr_3$	HBr aqueous solution	Visible light ($\lambda \geq 400$ nm), 300 W	13.3 μmol g^{-1} h^{-1}	20 h	[87]
		$Cs_2AgBiBr_6$/N-C	HBr aqueous solution	Visible light ($\lambda \geq 420$ nm), 300 W	380 μmol g^{-1} h^{-1}	24 h	[88]
		$Cs_2AgBiBr_6$/rGO	HBr aqueous solution	Visible light ($\lambda \geq 420$ nm), 300 W	48.9 μmol g^{-1} h^{-1}	120 h	[89]
		$Cs_2AgBiBr_6$/MoS_2	HBr aqueous solution	Visible light ($\lambda \geq 420$ nm), 300 W	87.5 μmol g^{-1} h^{-1}	500 h	[90]
		$MAPbBr_{3-x}I_x$/Pt	HI/HBr aqueous solution	Visible light ($\lambda \geq 420$ nm), 300 W	2604.8 μmol g^{-1} h^{-1}	30 h	[78]
		$CsPbBr_{3-x}I_x$/Pt	HI/HBr aqueous solution	Visible light ($\lambda \geq 420$ nm), 300 W	1120 μmol g^{-1} h^{-1}	50 h	[91]

(Continues)

26379368, 2024, 11, Downloaded from https://onlinelibrary.wiley.com/doi/10.1002/cey2.500, Wiley Online Library on [04/09/2026]. See the Terms and Conditions (https://onlinelibrary.wiley.com/terms-and-conditions) on Wiley Online Library for rules of use; OA articles are governed by the applicable Creative Commons License

TABLE 1 (Continued)

Strategy	Reaction types	Photocatalyst	Reaction medium	Light source	Activity	Stability	References
Core-shell structure	Photodegradation of RhB	$CsPbBr_3$/$CsPb_2Br_5$@SiO_2	Aqueous solution	Visible light (300 W, 3.8 mW cm^{-2})	Conversion: 97.4% (80 min)	2.7 h	[92]
	Photodegradation of antibiotic residues	$CsPbBr_3$@SiO_2	Aqueous solution	Visible light ($\lambda \geq 420$ nm), 300 W	Conversion: 75% (2 h)	4 h	[93]
	Photodegradation of RhB	$CsPbBr_3$/Sn-TiO_2	Aqueous solution	Solar light (1000 W m^{-2})	Conversion: 96.6% (30 min)	8 h	[94]
	CO_2 reduction	Bi-$CsPbCl_3$	CO_2/H_2O vapor	Full spectrum (300 W)	CO: 57 μmol g^{-1} h^{-1}	9 h	[95]
	CO_2 reduction	$CsPbBr_3$@Zn-ZIF-	CO_2/H_2O vapor	Solar light (100 W, 150 mW cm^{-2})	CH_4: 29.63 μmol g^{-1} h^{-1}	18 h	[96]
Functional protective layer	Polymerization	$MA_3Bi_2Br_9$-COF	Aqueous solution	Blue LED (10 W, 10 mW cm^{-2})	Conversion (97.5%, 21 h)	63 h	[88]
	CO_2 reduction	Co@$CsPbBr_3$/Cs_4PbBr_6	Pure water	Visible light irradiation ($\lambda > 420$ nm), 300 W	CO: 12 μmol g^{-1} h^{-1}	20 h	[97]
	CO_2 reduction	$CsPbBr_3$/UiO-$_{66}(NH_2)$	Water/EA	Visible light ($\lambda \geq 420$ nm), 300 W	CO: 8.21 μmol g^{-1} h^{-1} 1	36 h	[98]
	CO_2 reduction	$CsPbBr_3$/GDY	Water/EA	Visible light ($\lambda \geq 400$ nm), 300 W	CO: 10.2 μmol g^{-1} h^{-1}	36 h	[99]
	CO_2 reduction	$MAPbI_3$@PCN-221($Fe_{0.2}$)	Water/EA	Visible light ($\lambda \geq 400$ nm), 300 W	CO: 4.16 μmol g^{-1} h^{-1} 1 CH_4: 13 μmol g^{-1} h^{-1} 1	80 h	[100]
	CO_2 reduction	$CsPbBr_3$/MF	Pure water	Solar light irradiation, 300 W	CO: 29.13 μmol g^{-1} h^{-1} CH_4: 12.95 μmol g^{-1} h^{-1}	100 h	[73]
	H_2 generation	$CsPbBr_3$/TiO_2-Pt	Water/methanol	Visible light ($\lambda > 420$ nm), 300 W	H_2: 80 μmol g^{-1} h^{-1}	160 h	[101]
Water-stable MHP materials	H_2 generation	$Cs_2Pt_xSn_{1-x}Cl_6$	Aqueous solution	Solar light, 300 W	H_2: 16.11 μmol g^{-1} h^{-1}	4 h	[75]
	H_2 generation	$DMASnBr_3$/g-C_3N_4	Aqueous solution	Solar light (300–800 nm), 500 W m^{-2}	H_2: 1700 μmol g^{-1} h^{-1}	6 h	[74]
	H_2 generation	PEA_2SnBr_4/C_3N_4	Aqueous solution	Solar light, 500 W m^{-2}	H_2: 1613 μmol g^{-1} h^{-1}	6 h	[102]
	Photodegradation of MB				Conversion: 100% (40 min)		
	H_2 generation	$DMASnI_3$	Pure water	Solar light, 300 W	H_2: 0.64 μmol h^{-1}	20 h	[103]

26379368, 2024, 11, Downloaded from https://onlinelibrary.wiley.com/doi/10.1002/cey2.500, Wiley Online Library on [04/09/2026]. See the Terms and Conditions (https://onlinelibrary.wiley.com/terms-and-conditions) on Wiley Online Library for rules of use; OA articles are governed by the applicable Creative Commons License

TABLE 1 (Continued)

Strategy	Reaction types	Photocatalyst	Reaction medium	Light source	Activity	Stability	References
	Decarboxylation/ decarboxylation	$(HDA)_2PbI_4$	Aqueous solution	White LED (48 W)	Conversion: 98% (28 h)	28 h	[76]
	H_2 generation	$MA_2CuCl_2Br_2$	Pure water	Solar light, 150 W ($100\ mW\ cm^{-2}$)	H_2: 6 $\mu mol\ g^{-1}\ h^{-1}$	52 h	[104]

PEC system	Reaction types	MHP photoelectrode	Protective layer	Electrolyte	Light source	Efficiency	Stability	References
	O_2 evolution	$MAPbI_3$	Ni layer	0.1 M Na_2S aqueous solution	Solar light ($100\ mW\ cm^{-2}$)	$12\ mA\ cm^{-2}$ at 0 $V_{Ag/AgCl}$	1000 s	[105]
		$MAPbI_3$(TEA)	Ni layer	0.1 M Na_2S aqueous solution	Solar light ($100\ mW\ cm^{-2}$	$2.08\ mA\ cm^{-2}$ at 0 $V_{Ag/AgCl}$	30 min	[106]
		$MAPbI_3$	Ni layer	1 M boric acid/0.5 M KOH aqueous solution	Solar light ($100\ mW\ cm^{-2}$)	$17.4\ mA\ cm^{-2}$ at 1.23 V_{SHE}	1 h	[107]
		$MAPbI_3$	Ni layer/FM	1.0 M KOH aqueous solution	Solar light ($100\ mW\ cm^{-2}$)	$13\ mA\ cm^{-2}$ at 1.23 V_{RHE}	6 h	[108]
		$(5\text{-}AVA)_x(MA)_{1-x}PbI_3$	Carbon	1.0 M KOH aqueous solution	Solar light ($100\ mW\ cm^{-2}$)	$12.4\ mA\ cm^{-2}$ at 1.23 V_{RHE}	12 h	[109]
		Cs_2PtI_6	Ligands	KOH aqueous solution	Solar light ($100\ mW\ cm^{-2}$)	0.8 $mA\ cm^{-2}$ at 1.23 V_{RHE}	12 h	[110]
		$CsPbBr_3$	Carbon/graphite	0.1 M KNO_3 aqueous solution	Solar light ($100\ mW\ cm^{-2}$)	$2\ mA\ cm^{-2}$ at 1.23 V_{RHE}	30 h	[111]
	H_2 generation	$MAPbI_3$	FM (InBiSn alloy)	0.1 M borate aqueous solution	Solar light ($100\ mW\ cm^{-2}$)	$9.8\ mA\ cm^{-2}$ at 0 V_{RHE}	1 h	[112]
		$CsPbBr_3$	FM (InBiSn alloy)	0.2 m Na_2HPO_4/NaH_2PO_4 aqueous solution	Solar light ($100\ mW\ cm^{-2}$)	$1.2\ mA\ cm^{-2}$ at 0 V_{RHE}	1 h	[113]
		$MAPbI_3$	Ti foil	0.5 M H_2SO_4 aqueous solution	Solar light ($100\ mW\ cm^{-2}$)	$18\ mA\ cm^{-2}$ at 0 V_{RHE}	12 h	[114]
		CsMAFA	FM/AZO	0.5 M H_2SO_4 aqueous solution	Solar light ($100\ mW\ cm^{-2}$)	$14.3\ mA\ cm^{-2}$ at 0 V_{RHE}	18 h	[115]
		$MAPbI_3$	Ti foil	0.5 m H_2SO_4 aqueous solution	Solar light ($100\ mW\ cm^{-2}$)	$21.2\ mA\ cm^{-2}$ at 0 V_{RHE}	54 h	[116]
		FACs	Ti foil	1 M KOH aqueous solution	Solar light ($100\ mW\ cm^{-2}$)	$17.4\ mA\ cm^{-2}$ at 1.23 V_{RHE}	40 h	[117]

(Continues)

26379368, 2024, 11, Downloaded from https://onlinelibrary.wiley.com/doi/10.1002/cey2.500, Wiley Online Library on [04/09/2026]. See the Terms and Conditions (https://onlinelibrary.wiley.com/terms-and-conditions) on Wiley Online Library for rules of use; OA articles are governed by the applicable Creative Commons License

TABLE 1 (Continued)

PEC system	Reaction types	MHP photoelectrode	Protective layer	Electrolyte	Light source	Efficiency	Stability	References
	CO_2 reduction	$MAPbI_3$	FM (InBiSn alloy)	0.1 m $KHCO_3$ aqueous solution	Solar light (100 mW cm^{-2})	5.5 mA cm^{-2} at 0.6 V_{RHE}	1.5 h	[118]
		FAMA	$Cu_{96}In_4$ alloy	0.5 M $KHCO_3$ aqueous solution	Solar light (100 mW cm^{-2})	195 μA cm^{-2} at no applied bias	10 h	[119]
		CsFA	CoPc/CNT	0.5 M $KHCO_3$ aqueous solution	Solar light (100 mW cm^{-2})	15.5 mA cm^{-2} at −0.11 V_{RHE}	25 h	[120]
		CsFAMA	CoMTPP/CNT	0.5 M $KHCO_3$ aqueous solution	Solar light (100 mW cm^{-2})	100 μA cm^{-2} at no applied bias	67 h	[121]

Abbreviations: CNT, carbon nanotube; COF, covalent organic framework; CoMTPP, cobalt(II) meso-tetrakis(4-methoxyphenyl)porphyrin; Cs, cesium; DMA, dimethylammonium; FA, formamidinium; FM, Field's metal; GDY, graphdiyne; HDA, hexadecylammonium; MA, methylammonium; MHP, metal halide perovskite; PEA, phenylethylammonium; PEC, photoelectrochemical; RhB, rhodamine B.

aqueous solution and then perform the photocatalytic reaction.

This experiment was for the first time conducted by Wang et al.[77] in 2019. By adding the as-prepared $MAPbBr_3$ powder to an aqueous HBr solution, they found that the $MAPbBr_3$ fully dissolved at low concentration while forming the $MAPbBr_3$ precipitate when the concentration was greater than 0.24 mol L^{-1} (inset in Figure 8E). This is because high-concentration HBr solution provides a beneficial environment for the precipitation of $MAPbBr_3$ crystals, similar to that of $MAPbI_3$. Importantly, XRD patterns showed that the $MAPbBr_3$ remains stable in HBr aqueous solution for more than 3 months (Figure 8E). To further examine the photocatalytic property, the as-stabilized $MAPbBr_3$ was used for photocatalytic H_2 evolution in HBr solution. Under visible light irradiation ($\lambda > 420$ nm), an H_2 generation rate of 12.5 μmol g^{-1} h^{-1} was achieved on pure $MAPbBr_3$ photocatalyst. Further loading PEDOT:PSS and Ta_2O_5/Pt as electron- and hole-transporting motifs, respectively, the photoactivity was enhanced to 650 μmol g^{-1} h^{-1}, resulting in an apparent quantum efficiency of 16.4% for H_2 generation at 420 nm. Moreover, the photocatalytic performance showed negligible drops with three successive cycles (Figure 8F), confirming the well-maintained $MAPbBr_3$ phase. Building on this work, Guo et al.[87] reported the $CsPbBr_3$ nanocrystals for photocatalytic H_2 evolution (13.3 μmol g^{-1} h^{-1}) in saturated HBr aqueous under visible-light irradiation ($\lambda \geq 400$ nm). The $CsPbBr_3$ remained stable for 44 h of continuous irradiation. Similarly, Wang et al.[89] showed that the $Cs_2AgBiBr_6$ MHP decorated with graphene oxide (RGO) exhibited an H_2 productivity of 48.9 μmol g^{-1} h^{-1} in HBr aqueous solution under visible light irradiation ($\lambda \geq$ 420 nm), with excellent stability for 120 h continuous photocatalytic H_2 evolution. This method has also recently been adopted in $Cs_2AgBiBr_6$/N-C,[88] which enhanced the H_2 evolution rate to 380 μmol g^{-1} h^{-1}. Also, a discontinuous 500 h photocatalytic H_2 evolution reaction in HBr aqueous solution was achieved by Zhang et al.[90] in the $Cs_2AgBiBr_6/MoS_2$ system.

With a similar concept, when partial Br substituition by I in $MAPbBr_3$ forming $MAPbBr_{3-x}I_x$, the HBr/HI mixed aqueous solution should be suitable for stabilizing the $MAPbBr_{3-x}I_x$ for photocatalytic H_2 evolution reaction (Figure 8G). Specifically, Wu et al.[78] demonstrated that the $MAPbBr_{3-x}I_x$ sample with Pt as the cocatalyst exhibited the photoactivity of 2604.8 μmol g^{-1} h^{-1} in HBr/HI mixed solution under visible irradiation ($\lambda \geq 420$ nm) (Figure 8H), where the HI/HBr volume ratio plays a key role in stabilizing $MAPbBr_{3-x}I_x$ and thus the ultimate photoactivity. Additionally, $MAPbBr_{3-x}I_x$/Pt

26379368, 2024, 11, Downloaded from https://onlinelibrary.wiley.com/doi/10.1002/cey2.500, Wiley Online Library on [04/09/2026]. See the Terms and Conditions (https://onlinelibrary.wiley.com/terms-and-conditions) on Wiley Online Library for rules of use; OA articles are governed by the applicable Creative Commons License

showed excellent stability with negligible reduction in the photoactivity after 5 repeated cycles (Figure 8I). XRD and SEM results further confirmed that the material presents negligible changes in both structure and morphology after 30 h of H_2 evolution reaction. A similar result was also reported by Guan et al. for $CsPbBr_{3-x}I_x$ material.[91] Their study showed the $CsPbBr_{3-x}I_x$/Pt photocatalyst exhibited an H_2 evolution rate of 1120 $\mu mol\ g^{-1}\ h^{-1}$ under visible light irradiation ($\lambda \geq 420$ nm), with high stability during the 50 h of testing.

To sum up, the universality of the dynamic equilibrium approach has been demonstrated to be a promising strategy for photocatalytic H_2 production over MHP-based composites in aqueous media. However, since the experiments are performed in an MHP-saturated aqueous haloacid HX (X = Br and I), the strong acidity and corrosive ability of HX make the operational conditions harsh and dangerous and also prevent utilizing some cocatalysts which are not stable in HX. Besides, during the reaction process, the halide X^- will be oxidized into X_3^-, so additional reducing agents (such as H_3PO_2) are required to regenerate X^-, resulting in a rise in the cost and limiting the large-scale applicability. On the other hand, although many studies intentionally improve the photoactivity of MHP photocatalysts by loading cocatalysts or constructing heterojunctions, the underlying mechanisms of the contact between MHPs and metal cocatalysts or another semiconductor are unclear since the MHPs powder will dissolve and reprecipitate. Also, the H_2 evolution ability is still relatively low. Therefore, more alternative MHP-based H_2 generation routes still need to be explored.

4.2 | Physical protection

As clarified above, the strong acidity of halogen acid limits the further development of MHP photocatalysis. Besides, this method is confined to H_2 generation but cannot be extended to other reaction systems such as CO_2 reduction, organic transformation, and pollutant degradation. In this regard, extra effort should be devoted to developing more versatile approaches to moving MHP-based photocatalysis forward. Among various potential approaches, physical protection by encapsulating MHPs with water-resistant protective materials is a simple and straightforward method. Furthermore, different architectures (core-shell, heterojunction, etc.) and encapsulation materials (polymers, monodispersed capping agents, functional materials, surface ligands, etc.) can be adopted, which significantly broadens the ranges of the operability. Here, some powerful technologies that can help to improve the stability of MHPs will be introduced.

4.2.1 | Core-shell structure

Constructing a core-shell structure such as an oxide that serves as a protective shell with near-perfect coverage could protect MHPs from water, thus improving the stability of MHPs. This was confirmed experimentally by Li et al.[122] in 2017: they synthesized nearly monodisperse $CsPbBr_3/TiO_2$ core-shell nanocrystals through encapsulating colloidal $CsPbBr_3$ with titanium precursor (Figure 9A). The $CsPbBr_3/TiO_2$ core-shell samples were stable in water maintaining optical property for at least 3 months (Figure 9B). Inspired by this work, more MHP systems are designed and synthesized for photocatalysis in aqueous media. For instance, Li et al.[94] reported the core-shell structured $CsPbBr_3$/Sn-TiO_2 (Sn-doped TiO_2) enables long-term stability in water system. When the hybrid was applied to photocatalytic degradation of rhodamine B (RhB) in an aqueous solution under simulated solar light irradiation, the catalytic efficiency reached 96.6% in 30 min (Figure 9C), which is much higher than that of $CsPbBr_3/TiO_2$ nanocrystals and pure TiO_2. Recycling tests showed that the samples can work in water for more than 8 h. To further test the stability of this material, the sample was immersed in water and monitored. The absorbance property of the sample was maintained well with a slight drop in intensity after 20 days (Figure 9D), indicating the high stability of $CsPbBr_3$/Sn-TiO_2 in water.

Following these reports, more studies with the same strategy have been reported. For example, Gao et al.[93] synthesized a core-shell $CsPbBr_3@SiO_2$ for photodegradation of antibiotic residue in water under visible light irradiation ($\lambda \geq 420$ nm). Xie et al.[92] reported the $CsPbBr_3$/$CsPb_2Br_5@SiO_2$ sample dispersed in an aqueous solution for photocatalytic degradation of RhB. Similarly, Kong et al.[96] showed that the core-shell structured $CsPbBr_3$/Zn- and Co-based zeolitic imidazolate frameworks, $CsPbBr_3$@Zn-ZIF-8 and $CsPbBr_3$@Co-ZIF-67, exhibit improved humidity stability in a CO_2/water vapor reaction media. Also, Bi-doped $CsPbCl_3$ nanocrystal material with a core-shell structure against strong moisture was reported for photocatalytic CO_2 reduction.[95] Beyond these, excellent stability was also achieved for $CsPbBr_3/CsPb_2Br_5$[67] and $CsPbBr_3$/CdS[123] core-shell structures although they are still not used for photocatalysis.

To summarize, designing core-shell structures to minimize the contact between MHPs and water has been shown to be powerful for conducting photocatalytic reactions in aqueous media. Compared to traditional semiconductors, core-shell MHPs are still in their infancy. Although core-shell configuration has a very strong potential against water degradation, it remains quite challenging due to the inherent soft ionic nature of

26379368, 2024, 11, Downloaded from https://onlinelibrary.wiley.com/doi/10.1002/cey2.500, Wiley Online Library on [04/09/2026]. See the Terms and Conditions (https://onlinelibrary.wiley.com/terms-and-conditions) on Wiley Online Library for rules of use; OA articles are governed by the applicable Creative Commons License

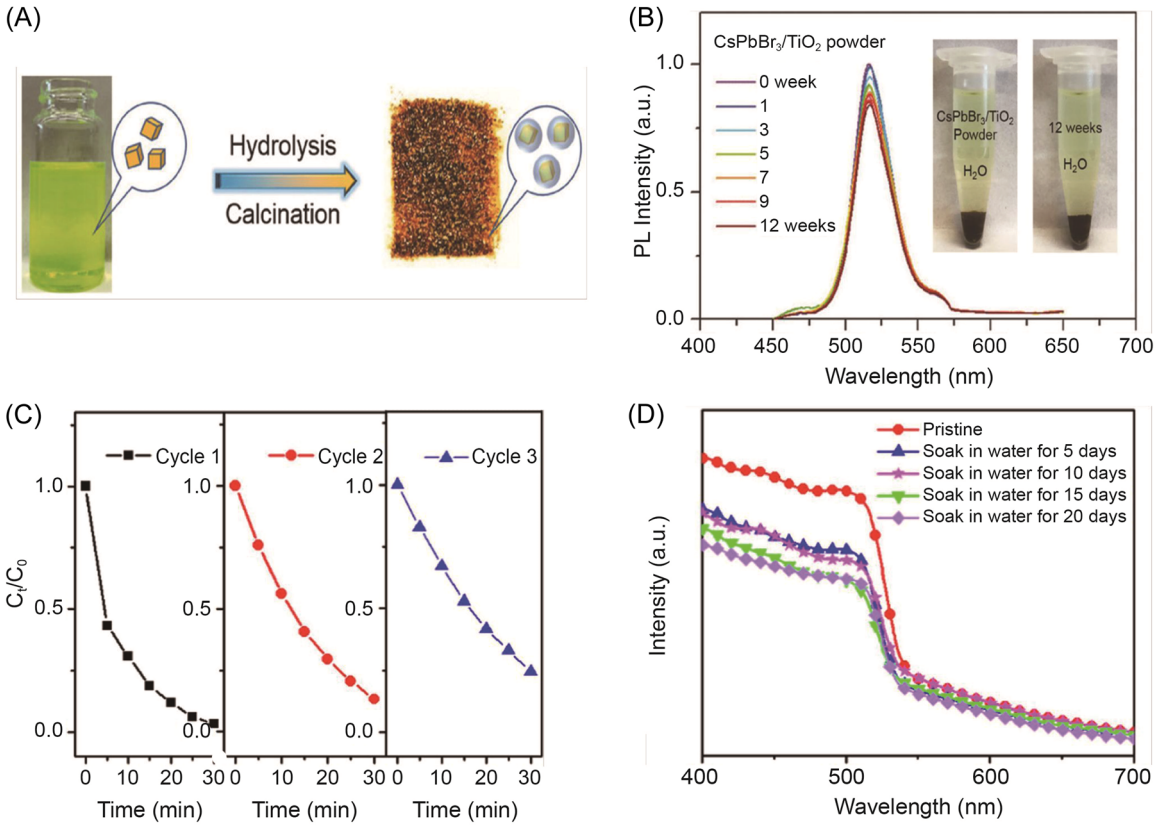


FIGURE 9 (A) Schematic illustration of the core-shell $CsPbBr_3/TiO_2$ nanocrystals. (B) The PL spectra of core-shell $CsPbBr_3/TiO_2$ sample after immersing in water for 12 weeks. Inset shows their optical images ([A and B] Reproduced with permission: Copyright 2017, Wiley-VCH[122]). (C) Cycling photocatalytic testing of core-shell structured $CsPbBr_3$/Sn-TiO_2 and (D) their absorption spectra after soaking in water for 20 days ([C and D] Reproduced with permission: Copyright 2022, Elsevier[94]).

MHPs. For example, the direct growth of shells on top of MHPs is always difficult. Besides, choosing the ideal shells with near-perfect lattice mismatch to MHPs is another tricky job. On the one hand, the shell material should serve as a physical barrier against water; on the other hand, it calls for promoting the charge transfer and separation at the interface to boost the photocatalytic performance of MHPs. Overall, there are some criteria that can be taken into consideration when adopting this method: (1) selecting potential shell materials and establishment of the band alignments, (2) evaluating the transparency of the shell material to make sure that the core material can be excited by the light source (such as visible light), (3) minimizing lattice mismatch between MHP and shell candidates on a case-by-case basis, and (4) constructing the core-shell structure using a suitable synthesis approach.

4.2.2 | Functional protective layer

Considering the challenges of core-shell structure, exploring more facile approaches is an easy solution, such as encapsulating MHPs with mechanically robust and stable functional protective layer. It should be noted that with similar materials such as TiO_2, metal-organic frameworks (MOFs), and covalent organic frameworks (COFs), they can be designed and synthesized as the shell of core-shell structure or generally functional protective layer, with the same goal for stabilization. Here we will focus on the latter one. So far, various encapsulation materials (organic polymers, MOFs, COFs, inorganic oxides, etc.) have been employed to enhance the stability of MHPs while maintaining their optical properties.

For instance, Zhu et al.[124] reported that the $MA_3Bi_2Br_9$ encapsulated by COFs exhibits good water resistance (Figure 10A). When applied to the polymerization of oligo-(ethylene glycol) methyl ether acrylate in pure deionized water under blue LED irradiation, 97.5% conversion over $MA_3Bi_2Br_9$-COF was achieved after 21 h irradiation. By contrast, pure $MA_3Bi_2Br_9$ without COF did not result in any polymerization due to the fast decomposition of $MA_3Bi_2Br_9$. Encouragingly, the $MA_3Bi_2Br_9$-COF sample can be reused for the photo-polymerization for three cycles without a significant

26379368, 2024, 11, Downloaded from https://onlinelibrary.wiley.com/doi/10.1002/cey2.500, Wiley Online Library on [04/09/2026]. See the Terms and Conditions (https://onlinelibrary.wiley.com/terms-and-conditions) on Wiley Online Library for rules of use; OA articles are governed by the applicable Creative Commons License

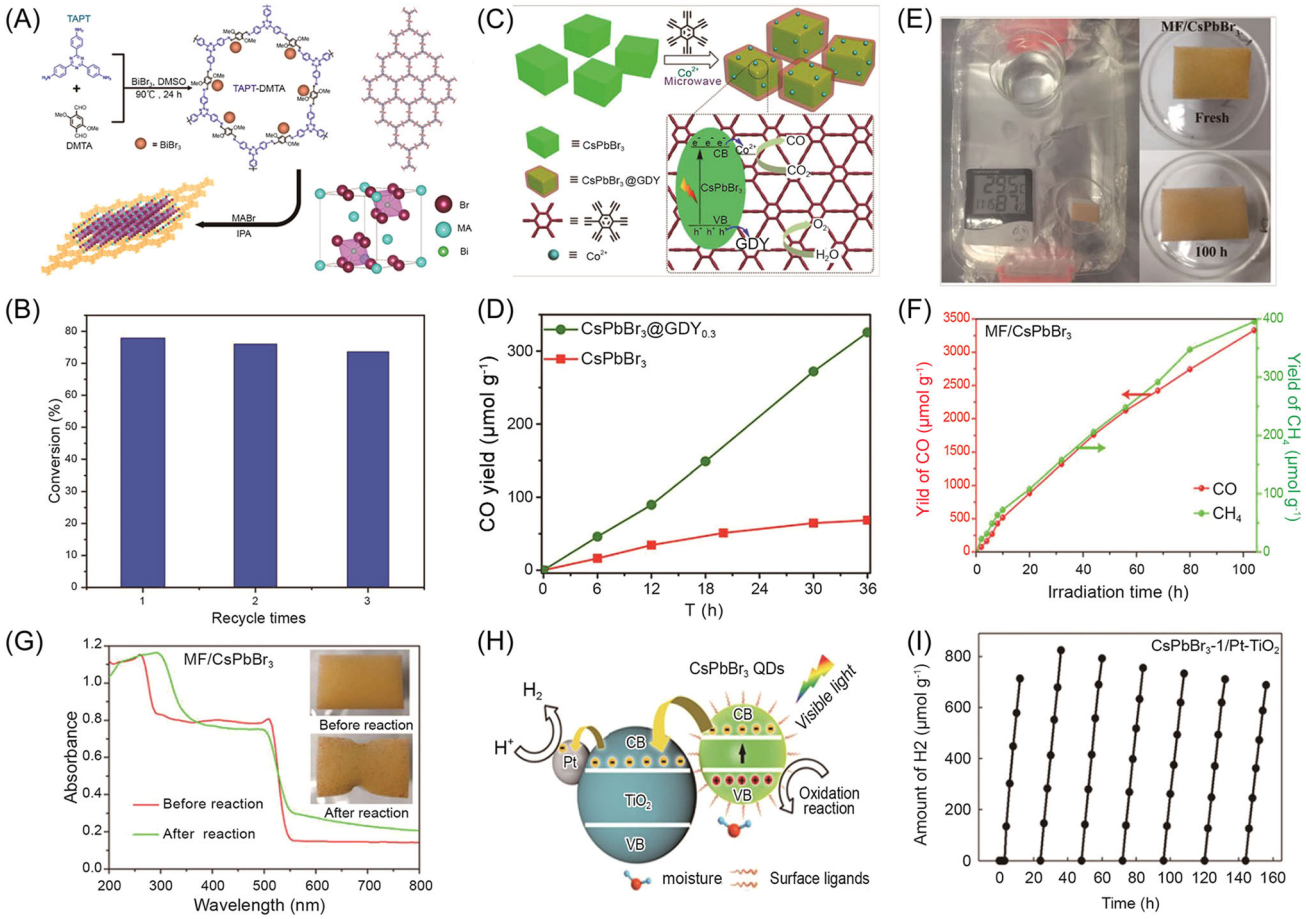


FIGURE 10 (A) Scheme of the in situ synthesis of $MA_3Bi_2Br_9$-COF composites and (B) recycling tests for polymerizing oligo-(ethylene glycol) methyl ether acrylate in water ([A and B] Reproduced with permission: Copyright 2022, American Chemical Society[124]). (C) Schematic illustration of the synthesis of $CsPbBr_3$@GDY and its application in photocatalysis. (D) Stability tracking of photocatalytic CO_2 reduction over $CsPbBr_3$@GDY composite ([C and D] Reproduced with permission: Copyright 2020, American Chemical Society[99]). (E) Photographs of $CsPbBr_3$/MF stored at ambient environment with 90 ± 5% relative humidity after 100 h. (F) Photocatalytic CO_2 reduction performance and (G) absorption spectrum of $CsPbBr_3$/MF in pure water under continuous light irradiation for 104 h ([E–G] Reproduced with permission: Copyright 2021, Wiley-VCH[73]). (H) Schematic illustration of the H_2 evolution over $CsPbBr_3$/Pt-TiO_2 and (I) the stability test of the sample in continuous operation ([H and I] Reproduced with permission: Copyright 2019, Wiley-VCH[101]). COF, covalent organic framework; GDY, graphdiyne.

compromise in photocatalytic performance (Figure 10B). XRD result showed the well-maintained structural integrity after the recycling tests, originating from the hydrophobic COF shell. This work showcases the potential of COFs as effective shields to protect the MHPs from degradation. Following this report, MOF-based encapsulation method was also adopted for photocatalytic applications. More specifically, Fe-porphyrin-based MOF was used to encapsulate $MAPbI_3$ quantum dots,[100] which showed a significantly enhanced water stability for photocatalytic CO_2 reduction under visible light irradiation in a water/ethyl acetate (EA) medium. Note that as an organic-inorganic hybrid MHP, $MAPbI_3$ is very unstable in water. The $MAPbI_3$/MOF sample exhibited high CO and CH_4 yields as well as remarkable stability over 80 h, confirming the benefits of the MOF encapsulation. In a similar fashion, UiO-66(NH_2)-MOF encapsulated $CsPbBr_3$ quantum dots were synthesized by Wan et al.[98] to enhance the photocatalytic performance and the stability of $CsPbBr_3$ for photocatalytic CO_2 reduction in an EA/water medium.

Next to the robust COF/MOF materials, a new carbon derivative, graphdiyne (GDY), with a 2D planar network structure was synthesized by Su et al. as the outer encapsulating layer. They constructed a $CsPbBr_3$/GDY structure for photocatalytic CO_2 reduction in a water-containing system (Figure 10C).[99] Benefiting from the physical barrier of GDY, the $CsPbBr_3$/GDY photocatalyst delivers improved stability, and no obvious drop in CO evolution for $CsPbBr_3$@GDY sample is observed after 36 h of photocatalytic reaction (Figure 10D). Importantly, the thin GDY layer not only serves as encapsulation material

26379368, 2024, 11, Downloaded from https://onlinelibrary.wiley.com/doi/10.1002/cey2.500, Wiley Online Library on [04/09/2026]. See the Terms and Conditions (https://onlinelibrary.wiley.com/terms-and-conditions) on Wiley Online Library for rules of use; OA articles are governed by the applicable Creative Commons License

to improve the stability of $CsPbBr_3$ but also acts as a hole transfer layer to facilitate the charge separation in $CsPbBr_3$ and, therefore, minimize electron-hole recombination, resulting in a high yield of 10.2 $\mu mol\ g^{-1}\ h^{-1}$ for photocatalytic CO_2 conversion to CO compared to pure $CsPbBr_3$ (3.3 $\mu mol\ g^{-1}\ h^{-1}$). This work shows the great promise of GDY as a protection layer, which offers a guideline for exploring new water-proof materials. For example, Mu et al.[97] constructed $Co@CsPbBr_3/Cs_4PbBr_6$ with hexafluorobutyl methacrylate serving as a water-proof layer for photocatalytic CO_2 reduction in pure water under visible light irradiation ($\lambda > 420$ nm), and 12 $\mu mol\ g^{-1}\ h^{-1}$ of CO yield was achieved. Additionally, the $Co@CsPbBr_3/Cs_4PbBr_6$ material dispersed in water after 100 h still exhibits good stability. Recently, a similar mechanism was proposed for the melamine foam (MF)/$CsPbBr_3$ system,[73] where the $CsPbBr_3$/MF presents long-term stability when exposed to a high relative humidity ($90 \pm 5\%$) environment for 100 h (Figure 10E). When it was applied to the photoreduction of CO_2 in pure water, the optimal $CsPbBr_3$/MF sample delivered the CO and CH_4 yields of 29.13 and 12.95 $\mu mol\ g^{-1}\ h^{-1}$, respectively, and the photoactivity showed insignificant decrease after continuous reaction for 104 h (Figure 10F). Due to the enhanced water resistance of the sample, no obvious variations in structural (XRD) and optical properties (absorbance, Figure 10G) were observed. These works open a boulevard for practical artificial CO_2 photoreduction using MHP-based photocatalysts in aqueous solutions.

Apart from the introduction of alien encapsulation materials, engineering long-chain organic ligands in the MHP quantum dots is another effective strategy, where the increased surface hydrophobicity can reduce the interaction between MHP and water molecules. For instance, Wang's group showed that surface modification is powerful to stabilize the $CsPbBr_3$ quantum dots from moisture corrosion while maintaining the efficient charge transfer for photoredox reaction.[101] By rational control of the termination during the process of $CsPbBr_3$ synthesis, a surface ligand stabilized $CsPbBr_3/TiO_2$ composite was developed for photocatalytic H_2 production in a mixed water/methanol vapor medium (20 vol%) under visible light irradiation ($\lambda > 420$ nm) (Figure 10H). With the Pt nanoparticles as the cocatalysts, the optimized $CsPbBr_3$/Pt-TiO_2 photocatalyst exhibited a catalytic activity of about 80 $\mu mol\ g^{-1}\ h^{-1}$. Impressively, cycling tests showed no attenuated photoactivity over the $CsPbBr_3$/Pt-TiO_2 after continuous H_2 evolution for 160 h (Figure 10I), which is supported by the powder XRD patterns of the sample after photocatalytic reaction, confirming the stability of $CsPbBr_3$/Pt-TiO_2. This work presents a significant step in engineering surface ligands to protect MHP from degradation in moisture in photocatalytic applications.

Overall, encapsulating or wrapping the MHPs with waterproof materials is an appealing approach to prevent the undesirable physical degradation of MHP-based photocatalysts. Due to a wide variety of choices, this strategy has been widely adopted to date. From the perspective of photocatalysis, the photogenerated charge carriers need to be separated and transferred to participate in the photoredox reactions. To kill two birds with one stone, the selection of the encapsulation materials is of great importance, and this is always ignored without being clearly identified. Therefore, the development of encapsulation materials with suitable conductivity, hydrophobicity, porous structures, band energies, and chemical interactions would bring a new blueprint for encapsulation technology. For instance, encapsulating $CsPbBr_3$ quantum dots into polypyrrole conducting polymer has been conducted to present simultaneously excellent stability for 30 days in water and efficient charge transport property.[125] On the other hand, although encapsulation layer crafting in MHP-based photocatalysts has been widely used for CO_2 reduction and H_2 evolution, the applications in organic transformations and pollutant degradation have not been fully investigated.

4.2.3 | PEC system

In addition to the powder suspension catalysts, fabricating MHP thin films acting as active layers for the photoelectrodes has attracted much attention. Similarly, to realize the PEC process, the stability issue is the first and key factor that needs to be solved due to the extreme sensitivity of MHPs toward water. Fortunately, inspired by the MHP-based solar cell configurations, some impressive studies with excellent operational stability have been reported. Generally, a separated or integrated Photovoltaic (PV)-PEC configuration can be designed, depending on whether the MHPs are immersed in an aqueous solution. Here, we mainly focus on the latter one, highlighting the applications in PEC water oxidation, H_2 generation, and CO_2 reduction with some selected examples.

4.2.4 | PEC water oxidation

In 2015, Da et al.[105] first reported an $MAPbI_3$-based photoanode for PEC water oxidation. With a Ni layer serving as both a waterproof shield and cocatalyst, the $MAPbI_3$/Ni photoanode exhibited a photocurrent density of 12 $mA\ cm^{-2}$ at 0 V (vs. Ag/AgCl) in 0.1 M Na_2S aqueous solution under solar irradiation. However, the sacrificial agent with S^{2-} has been reported that it

26379368, 2024, 11, Downloaded from https://onlinelibrary.wiley.com/doi/10.1002/cey2.500, Wiley Online Library on [04/09/2026]. See the Terms and Conditions (https://onlinelibrary.wiley.com/terms-and-conditions) on Wiley Online Library for rules of use; OA articles are governed by the applicable Creative Commons License

contribute to photocurrent density.[126] Besides, the photocurrent density decreased to 20% after 1000 s due to the degradation of $MAPbI_3$. To improve the photocurrent density and stability of the MHPs, much effort has been made in the following years.

For example, Wang et al.[106] introduced a Ni protective layer and surface-functionalized treatment with hydrophobic alkyl ammonium cations to $MAPbI_3$ against water molecules, leading to a stable photocurrent of 2.08 mA cm^{-2} for 30 min. Hoang et al.[107] showed that a thick pinhole-free hole transport layer (spiroMeOTAD) could enhance the stability of $MAPbI_3$ photoelectrode, thus extending the photoelectrode lifetime to around 1 h. Nam et al.[108] utilized metal encapsulation comprising Field's metal (FM) and Ni catalyst layer that acted as both a protective layer and electrocatalyst in $MAPbI_3$-based system, yielding a stable photocurrent of 13 mA cm^{-2} after 6 h. Besides the $MAPbI_3$-based photoelectrodes, a similar strategy has also been used for the $(5\text{-AVA})_x(MA)_{1-x}PbI_3$ (photocurrent density: 12.4 mA cm^{-2} at 1.23 V_{RHE}; stability: 12 h (70%))[109] and Cs_2PtI_6 (photocurrent density: 0.8 mA cm^{-2} at 1.23 V_{RHE}; stability: 12 h (~100%))[110] PEC systems.

Although these studies have achieved much progress, the relatively short-term stable photoelectrodes within the PEC system limit their further development. Therefore, it is still highly desirable to explore more protection approaches to build robust PEC devices. Among various materials, carbon-based materials with high conductivity and low-cost merits are a good choice, which not only insulate MHPs from water but also can serve as a charge transport layer to facilitate electron–hole separation. Also, to meet the requirement of water splitting, MHPs with wider bandgap (such as $CsPbBr_3$, $E_g = 2.3$ eV) have been exploited. For example, Poli et al.[111] employed a graphite sheet (GS) and a mesoporous carbon (m-c) scaffold to encapsulate $CsPbBr_3$, forming a $TiO_2/CsPbBr_3$/m-c/GS planar solar cell device configuration (Figure 11A). Benefiting from the protection of hydrophobic GS and thick m-c layer, the $CsPbBr_3$-based photoanode achieved excellent stability for 30 h at 1.23 V_{RHE} in aqueous electrolyte under constant simulated solar light illumination (Figure 11B), with a steady photocurrent above 2 mA cm^{-2}. Note that the relatively low photocurrent density in this study could be improved via composition engineering of MHPs, such as $FA_{0.83}Cs_{0.17}Pb(I_{0.8}Br_{0.2})_3$, $FAMA_{0.22}Cs_{0.07}Pb_{1.32}I_{3.27}Br_{0.66}$, and so on. Besides, the combination of tandem devices on photoanode/photocathode with more protection layers for PEC overall water splitting can both realize high performance and long-term stability goals, which is summarized in Table 1.

4.2.5 | PEC H_2 generation

In parallel with PEC water oxidation for O_2 evolution, the H_2 generation via PEC water splitting has attracted continuous attention. Especially to achieve the goal of carbon neutrality, developing sustainable clean energy like H_2 to replace traditional polluting fossil fuels is the key component. Due to the fantastic optoelectronic properties of MHP materials, employing the MHPs for PEC H_2 generation is an inevitable practice. Note that compared with traditional semiconductors, MHPs generally have relatively high CB positions (Figure 3B), therefore endowing enough redox potential for H_2 production (H^+/H_2, 0 V_{NHE}).

Since the water-sensitive characteristics of MHPs, unitizing additional protection layers such as bulk materials (e.g., FM and Ti foil) to avoid direct contact between MHP and water is the prerequisite. In 2016, Reisner's group first demonstrated the metal encapsulation technique using a water-resistant fusible InBiSn alloy (FM) to protect $MAPbI_3$-based photocathode in a single device capable of stable PEC H_2 generation in water (Figure 11C).[112] As a result, a record photocurrent density of −9.8 mA cm^{-2} at 0 V_{RHE} was obtained. Encouragingly, the isolated photoelectrodes from water showed remarkable stability, retaining over 80% of initial photocurrent for about 1 h under continuous solar irradiation (Figure 11D). Following this work, the same concept, that is, using FM as the physical barrier to shield MHPs for PEC H_2 evolution, has been used to $CsPbBr_3$,[113] $MAPbI_3$,[114] and CsMAFA triple cations[115] based photocathode, where the current reached −14.3 mA cm^{-2} at 0 V_{RHE} and the stability retained 18 h without drops in photocurrent density.

Next to FM, Ti foil has been employed as a protective material since its cheap, robust, and chemically stable benefits. For example, Li's group reported a sandwich-like $MAPbI_3$ photocathode (NiO/$MAPbI_3$/phenyl-C61-butyric acid methyl ester, PCBM),[114] using Ti foil as the protection layer. The fabricated $MAPbI_3$ photocathode delivered a photocurrent density of −18 mA cm^{-2} at 0 V_{RHE} in 0.5 M H_2SO_4 under simulated solar illumination, with a solar-to-fuel conversion efficiency of 7.63%. Impressively, the photocathode exhibited a stable PEC H_2 evolution for at least 12 h, confirming the benefits of the Ti foil. To take advantage of this merit, more studies with the same method for PEC water splitting have also been reported in $MAPbI_3$[106,107,116] and $FA_{0.83}Cs_{0.17}Pb(I_{0.8}Br_{0.2})_3$[117] photoelectrode active layers.

4.2.6 | PEC CO_2 reduction

As a greenhouse gas, CO_2 has been deemed as the main reason causing the temperature increase of our planet.

26379368, 2024, 11, Downloaded from https://onlinelibrary.wiley.com/doi/10.1002/cey2.500, Wiley Online Library on [04/09/2026]. See the Terms and Conditions (https://onlinelibrary.wiley.com/terms-and-conditions) on Wiley Online Library for rules of use; OA articles are governed by the applicable Creative Commons License

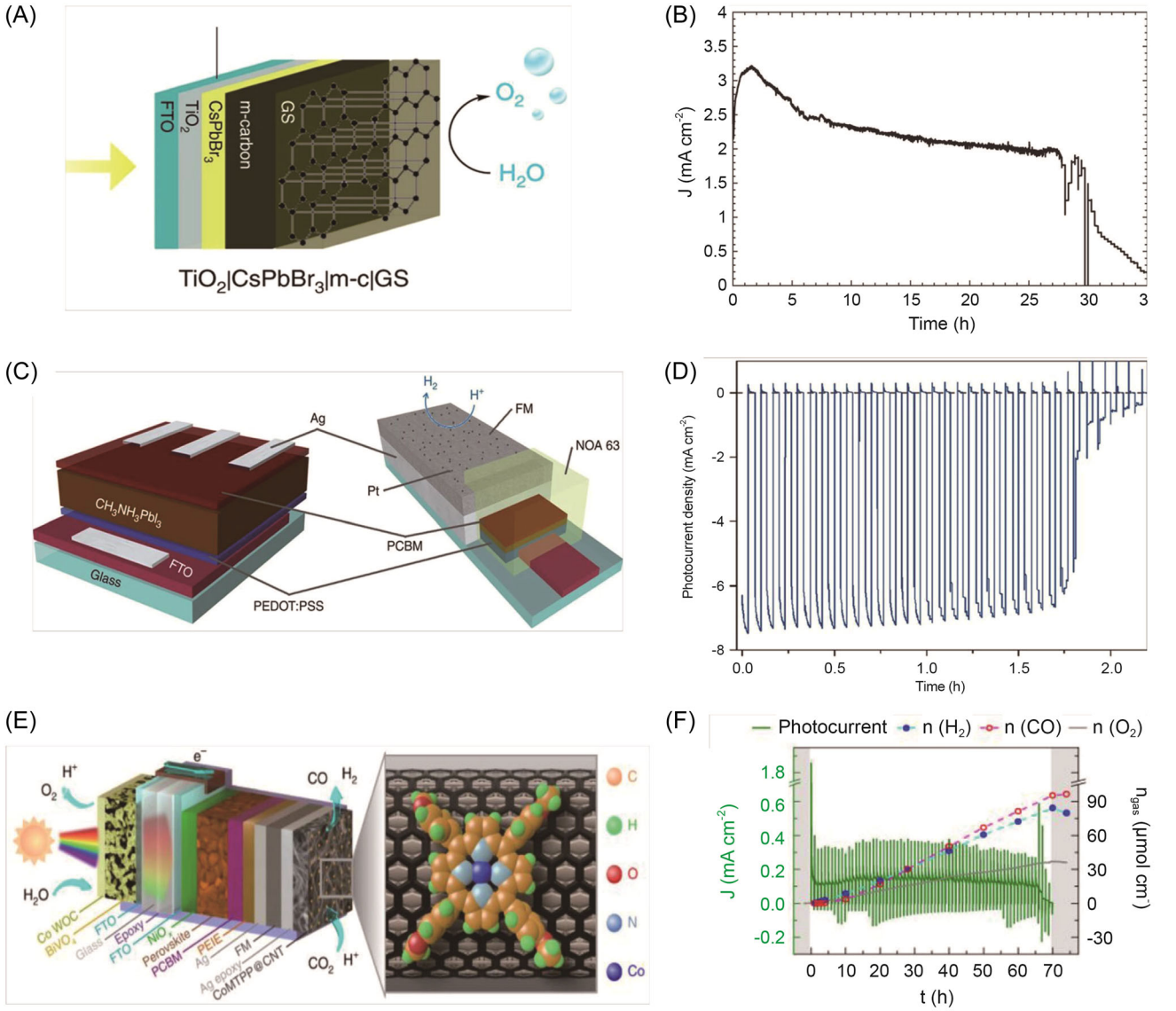


FIGURE 11 (A) Schematic illustration of $CsPbBr_3$ photoanode for PEC O_2 evolution and (B) stability test at 1.23 V_{RHE} under 1 sun irradiation in water ([A and B] Reproduced with permission: Copyright 2019, Nature[111]). (C) Schematic illustration of the $MAPbI_3$ photocathode for PEC H_2 evolution and (D) the chronoamperometric trace recorded at 0 V_{RHE} in water ([C and D] Reproduced with permission: Copyright 2016, Springer Nature[112]). (E) Schematic illustration of MHP-based photocathode for PEC CO_2 reduction and (F) stability measurement under 0.1 sunlight irradiation ([E and F] Reproduced with permission: Copyright 2019, Springer Nature[121]). MHP, metal halide perovskite; PEC, photoelectrochemical.

Converting CO_2 into energy fuels (CO, CH_4, HCOOH, HCHO, CH_3OH, etc.) is not only meaningful for chemical fuel generation but can also alleviate climate change.[127] Recently, MHPs have been employed as promising photocatalysts for CO_2 reduction. Until now, the CO_2 reduction experiments using MHP photocatalysts are mainly carried out in a low polarity solvent such as ethyl acetate, while in aqueous media, realizing such experiments is still challenging. To solve this issue, crafting MHP-based photoelectrode via covering MHP materials with conductive and water-proof layers for PEC CO_2 reduction is promising.

For instance, Chen et al.[118] showed that by employing the In-Bi-Sn ternary alloys to protect the $MAPbI_3$, where its low melting point eutectic molten state will not damage the $MAPbI_3$ during coating, an efficient and stable photocathode PEC CO_2 conversion in aqueous solution was achieved. Besides as the protective layer, In, Bi, and Sn metals are HCOOH selective, which provided highly selective CO_2 to HCOOH conversion. As a result, this $MAPbI_3$ photocathode-based PEC system delivered a current density of 5.5 mA cm^{-2} at −0.6 V_{RHE}, and device stability over 1.5 h without a decrease under solar light irradiation was achieved. Following this report, an

26379368, 2024, 11, Downloaded from https://onlinelibrary.wiley.com/doi/10.1002/cey2.500, Wiley Online Library on [04/09/2026]. See the Terms and Conditions (https://onlinelibrary.wiley.com/terms-and-conditions) on Wiley Online Library for rules of use; OA articles are governed by the applicable Creative Commons License

FAMA-based MHP-$BiVO_4$ tandem device with bimetallic $Cu_{96}In_4$ alloy was also adopted,[119] where the buried MHP-$Cu_{96}In_4$ cathode showed robust, unaltered PEC activity at different solar intensities. The device showed a photocurrent density of 195 $\mu A\ cm^{-2}$ at no applied bias, with a solar-to-CO energy conversion efficiency of 0.19% and a selectivity of 75% for CO after 10 h irradiation under simulated sunlight without bias. Although these works demonstrate the feasibility of PEC CO_2 reduction using MHP photocathodes, the operational stability is still unsatisfactory. Thus, the quest for more stable PEC systems continues.

Utilizing carbon material is promising since it not only provides protection to the MHP light absorbers but also can facilitate electron transfer. In this regard, Li's group developed a carbon-encapsulated sandwich-like $(Cs_{0.15}FA_{0.85})Pb(I_{0.9}Br_{0.1})_3$ photocathode (device structure: FTO/NiO/MHP/PCBM/BCP/Cu/carbon plat) for PEC CO_2 reduction in aqueous solution.[120] With a CoPc molecular catalyst immersed in carbon nanotube (CNT), the photocathode displayed a photocurrent density of $-15.5\ mA\ cm^{-2}$ at $-0.11\ V_{RHE}$ in 0.5 M $KHCO_3$ solution under solar light illumination. Moreover, the photocathode remains stable during a continuous reaction over 25 h. Moreover, unbiased PEC CO_2 reduction was also achieved when coupling the photocathode with an amorphous Si photoanode in tandem, resulting in a solar-to-fuel energy conversion efficiency of 3.85%. Inspired by this work, Reisner's group recently constructed a standalone MHP-$BiVO_4$ PEC tandem device for bias-free CO_2 conversion (Figure 11E).[121] With the cobalt(II) meso-tetrakis(4-methoxyphenyl) porphyrin (CoMTPP) molecular catalyst immobilized on CNTs to protect the CsFAMA triple-cation MHP, reduction of CO_2 in water under solar irradiation with no applied bias resulted in simultaneous CO_2 reduction and waters splitting for solar syngas production, delivering solar-to-CO and solar-to-H_2 conversion efficiencies of 0.02% and 0.06%, respectively. Most importantly, the stability test showed that this system could be operated at photocurrents higher than 100 $\mu A\ cm^{-2}$ for 67 h (Figure 11F), suggesting that the design of a tandem device with suitable protective materials could be a promising strategy for achieving high PEC performance and long-term stability.

To sum up, compared to MHP-based powder photocatalysis, the PEC configurations offer the prospect of viable stability under real-world aqueous conditions and higher solar-to-fuels conversion efficiency. Despite the great promises, the PEC device systems generally rely on expensive materials and sophisticated architectures. Therefore, simplifying the fabrication techniques with cheaper materials is another appealing research direction to be developed. Besides, despite multiple protective layers with different properties that can be deposited onto the MHP photoelectrodes, the water molecules still can inevitably penetrate to destabilize the MHP, originating from the (photo)chemical corrosion of the embankments and gas bubble formation inducing mechanical stress and leakage. Thus, designing water-resistant robust protection materials, developing improved encapsulation technologies, and modifying the coating processes (such as the thickness of the protective layers) are effective routes to prolong the stability of MHP photoelectrodes. On the other hand, in addition to improving operational stability, increasing PEC efficiency is also a key objective. Selectively depositing robust electron- and hole-transporting materials with conductive cocatalyst layers on the top of MHP-based photoelectrodes to promote charge separation can be taken into consideration.

4.3 | Water-stable MHP materials

Although the above proposed several strategies indeed extended the operational time of MHP in an aqueous environment to some extent, developing intrinsically stable MHPs in water continues to be the desire. A growing interest in water-stable MHPs is fostering current research, which motivates the exploration of new materials. Encouragingly, some MHPs have been demonstrated to be stable in water so far. In this section, the recently developed MHPs enabling photocatalytic reactions in aqueous solutions will be summarized and discussed.

First, MHP materials such as $DMASnX_3$ (DMA = dimethylammonium, X = Br and I) with the relatively strong hydrophobicity of the DMA cation have been demonstrated to show impressive stability in water. For example, Romani et al.[74] reported that the $DMASnBr_3$ (Figure 12A) could act as a water-stable photocatalyst for photocatalytic H_2 generation in an aqueous solution (10% v/v triethanolamine). Under simulated solar light irradiation, the pure $DMASnBr_3$ exhibited an H_2 evolution rate of 6 $\mu mol\ g^{-1}\ h^{-1}$ after 6 h. To improve the photoactivity, C_3N_4 was introduced to form the $DMASnBr_3$/g-C_3N_4 composites. As a result, the optimal photocatalyst delivered an impressive H_2 production of 1700 $\mu mol\ g^{-1}\ h^{-1}$ (Figure 12B) with an apparent quantum yield of 6.6%. Moreover, structural (XRD and X-ray photoelectron spectroscopy (XPS)) and optical (absorbance) characterizations for the $DMASnBr_3$ sample before and after recovery from the aqueous solution further proved its excellent stability. Following this work, Tao's group also showed that the $DMASnI_3$ crystals exhibit excellent water stability for photocatalytic H_2 evolution

26379368, 2024, 11, Downloaded from https://onlinelibrary.wiley.com/doi/10.1002/cey2.500, Wiley Online Library on [04/09/2026]. See the Terms and Conditions (https://onlinelibrary.wiley.com/terms-and-conditions) on Wiley Online Library for rules of use; OA articles are governed by the applicable Creative Commons License

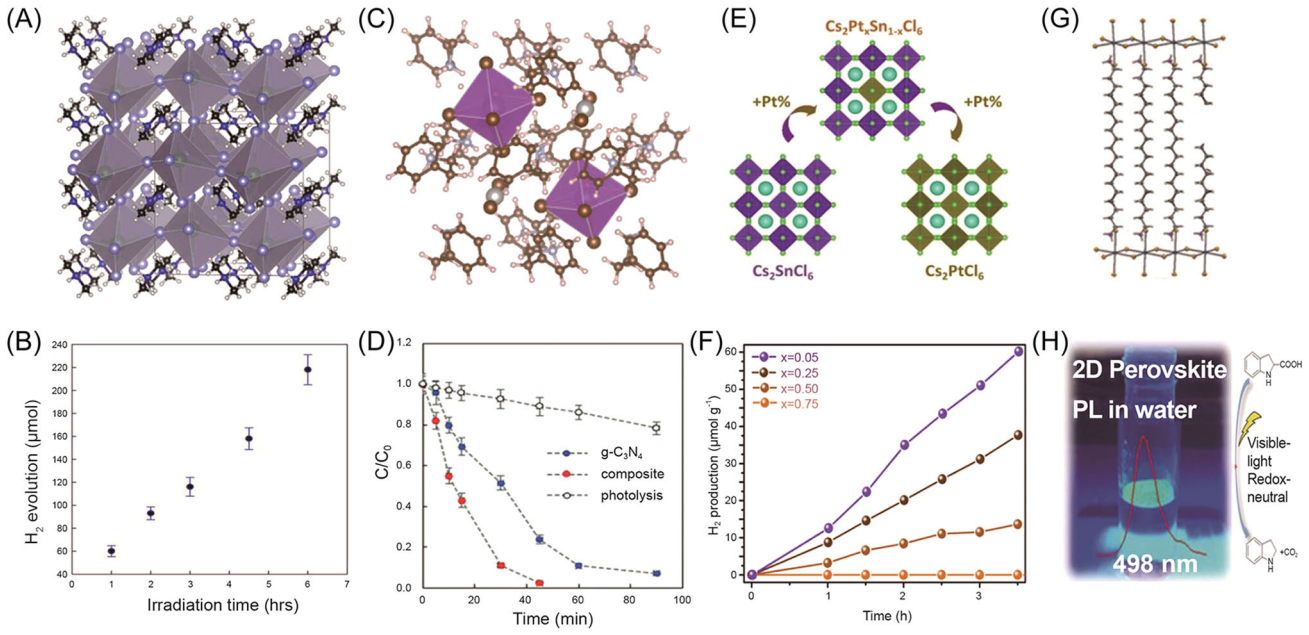


FIGURE 12 (A) Schematic illustration of $DMASnBr_3$ crystal structure. (B) H_2 evolution profile over time for 6 h using $DMASnBr_3$/g-C_3N_4 composite as the photocatalyst in an aqueous solution (10% v/v triethanolamine) ([A and B] Reproduced with permission: Copyright 2020, Wiley-VCH[74]). (C) Schematic representation of PEA_2SnBr_4 crystal structure. (D) Photocatalytic degradation of MB over PEA_2SnBr_4/g-C_3N_4 composites ([C and D] Reproduced with permission: Copyright 2020, Royal Society of Chemistry[102]). (E) Scheme of the crystal structure of $Cs_2Pt_xSn_{1-x}Cl_6$ and transformation relationship related to Cs_2SnCl_6 and Cs_2PtCl_6. (F) Photocatalytic H_2 generation over Pt/$Cs_2Pt_xSn_{1-x}Cl_6$ in water ([E and F] Reproduced with permission: Copyright 2021, Wiley-VCH[75]). (G) Crystal structure of $(HDA)_2PbI_4$. (H) Photographs of $(HDA)_2PbI_4$ suspended in water and its PL spectrum, together with the model reaction used in this work ([G and H] Reproduced with permission: Copyright 2019, Wiley-VCH[76]). DMA, dimethylammonium; HDA, hexadecylammonium; MB, methylene blue.

in pure deionized water.[103] Under full spectrum irradiation, the pure $DMASnI_3$ sample yielded an H_2 evolution rate of 0.64 μmol h^{-1} after 5 h, with good recycling property (5 cycles, 20 h in total). These studies pave the way to the realization of a new class of water-stable MHP photocatalysts.

Next to the DMA-based MHPs, a novel 2D phenylethylammonium (PEA)-based MHP, PEA_2SnBr_4 (Figure 12C),[102] has also been reported, showing impressive water-resistance by maintaining its crystal structure and optical properties when immersed in water. To examine its photocatalytic property, H_2 generation from water and organic pollutant degradation were performed simultaneously. Under solar light irradiation, the pure PEA_2SnBr_4 photocatalyst yielded an H_2 production of 4 μmol g^{-1} h^{-1} after 6 h continuous reaction, which is elevated to 1613 μmol g^{-1} h^{-1} after coupling with the C_3N_4 material. To further confirm the versatility of the PEA_2SnBr_4 material in different aqueous solutions, photocatalytic degradation of methylene blue (MB) was carried out. An analogous result in the efficiency of MB degradation is shown in Figure 12D, suggesting the good water resistance of the PEA_2SnBr_4. The discovery of this MHP allows us to explore more photocatalytic applications which will not be limited to organic solvents but will be also suited to various aqueous media.

Moreover, ion substitution has also been demonstrated to be an effective strategy. For example, Yin et al.[75] showed that the MHP single crystal ($Cs_2Pt_xSn_{1-x}Cl_6$, $0 \le x \le 1$) can be employed for H_2 generation in aqueous solution by substituting Sn^{4+} in Cs_2SnCl_6 with Pt^{4+} (Figure 12E). Under simulated solar light irradiation, the H_2 production rate of 16.11 μmol g^{-1} h^{-1} over pure $Cs_2Pt_{0.05}Sn_{0.95}Cl_6$ was obtained (Figure 12F). The optical properties of the material remained unchanged after being soaked in water for 4 h. Although this work offers a feasible method to develop water-stable MHP materials, it requires finding a suitable parent matrix (such as Cs_2SnCl_6) and an ion substitution (e.g., Pt^{4+}), making the whole process complex. Considering the diversity of the MHPs, designing hydrophobic cations as intercalating layers could be useful. This was demonstrated by Hong et al.[76] They showed that by incorporating the long-chained hexadecylammonium (HDA) between the metal halide nanosheets, a 2D hydrophobic $(HDA)_2PbI_4$ MHP (Figure 12G) could retain its crystal structure (XRD pattern) and optical properties (absorbance) in water. This is attributed to the long hydrophobic aliphatic HDA chains which intimately caused congestion in the inorganic layers in the MHP structure to avoid the entry of water molecules. To

26379368, 2024, 11, Downloaded from https://onlinelibrary.wiley.com/doi/10.1002/cey2.500, Wiley Online Library on [04/09/2026]. See the Terms and Conditions (https://onlinelibrary.wiley.com/terms-and-conditions) on Wiley Online Library for rules of use; OA articles are governed by the applicable Creative Commons License

explore the potential photocatalytic applications of $(HDA)_2PbI_4$, the sample was used for the photocatalytic decarboxylation and oxidative dehydrogenation reactions (Figure 12H). Under white LED irradiation (48 W), 98% indoline can be converted after 14 h. In addition, the photocatalyst can be reused for the reaction, and XRD and XPS showed the structure and elemental information (contents and oxidation states) of the sample after photocatalysis remained.

In addition to the above materials, $MA_2CuCl_2Br_2$ was also recently reported for vapor-phase photocatalytic water splitting with stability for up to 50 h.[104] Besides, other MHPs include $EtbtBi_2I_{10}$,[128] $C_{22}H_{18}N_2(PbI_3)_2$,[129] $OHNH_3PbI_2Cl$,[130] and $(DAO)Sn_2I_6$[131] have been claimed to be water-resistant MHP materials, while their potential applications in photocatalysis have not been explored.

Overall, several MHP materials have shown their great prospects in photocatalysis under water-based environments, while the quality still needs to be improved for practical applications. Table 1 summarizes the various strategies used to improve the stability of MHPs for performing the photoredox reactions in aqueous solutions. Although the progress of water-stable MHP-based photocatalysis is still in its infancy, the integration of multidisciplinary knowledge across materials science and theoretical calculations will rapidly develop this area, and hopefully, MHP photocatalysts with long-term water stability and high activity can be developed and play significant roles in photocatalysis.

5 | CONCLUSIONS AND PROSPECTS

Besides the traditional PV applications, MHP materials have recently emerged as promising photocatalysts. The past few years have witnessed the rapid development of MHPs for photocatalytic solar-to-chemical energy conversion, while the poor water stability of MHPs is considered the main bottleneck for their further development. However, for most photocatalytic reactions, the water environment is required, either as the solvent or as the reactant itself. On the other hand, water could be generated as a byproduct in some photoredox reactions. Thus, the photocatalytic solar-to-chemical energy conversion over MHPs in aqueous media should be achievable to meet the requirements of the practical applications. To fill the gap, tremendous efforts have been devoted to developing useful strategies to improve the stability of MHP materials for photocatalytic reactions in aqueous media. Despite great advancements achieved, it still encounters grand challenges before realizing its full potential toward practical applications. Based on current progress, some perspectives on future development are proposed.

First, exploring various precipitation–solubility equilibrium systems between MHPs and soluble ionic species should be concerned.[43] Currently, this method is only used in a saturated HX aqueous solution for H_2 generation, while it is anticipated that this strategy can be extended to other reaction systems (CO_2 reduction, organic synthesis, etc.). Once the dynamic stability of the MHPs in these applications can be achieved, it will open a boulevard toward practical applications. Therefore, more attention is encouraged to this research direction.

Second, novel protective layers or surface ligands for MHPs need to be developed by exploring various coating and synthesis methodologies. Before covering the photoelectrodes with functional materials, an in-depth understanding of coating approaches and their effect on the MHP materials is of great importance. For example, in a core-shell structure, a semiconducting or conducting shell should be considered, which could facilitate charge transfer via interface engineering or band alignment across the core-shell structures.[17] Furthermore, developing the surface ligands stabilizing MHPs that possess electron-donating or electron-withdrawing properties may contribute to the photoredox reactions.[43] While for the general functional layers (and PEC systems), besides the solution-based and evaporative growth methods, a combination of these two methods with solid-to-melt approaches is meaningful. Additionally, simplifying the complex device structure and reducing the use of expensive materials are anticipated.

Third, more water-stable MHP compounds should be explored. Tackling the problem at its roots undoubtedly is the most useful route. Considering the ionic nature of the MHPs, the process of discovery is very slow compared to the race for photocatalytic performance. It has been demonstrated that most 3D MHPs used today are very sensitive to water, while recent studies have demonstrated the water-stable ability of low-dimensional MHPs. Thus, more effort can be made to continue to examine this kind of MHPs; especially, the 2D MHPs such as A site with an organic cation like PEA and DMA and B site metal cation like Cu and Sn can be promising, with the aid of machine learning.

Fourth, comprehensive studies must be undertaken to better understand the mechanism of the degradation behaviors of the MHPs. With the same MHPs, some studies reported that they tend to be degraded easily once contacted with water, while others claimed that they can be stable in water. To fully reveal the true colors, some investigations can be focused on surface ligand-mediated stable property to figure out how the ligand assists in the stabilization, which may spur the innovation to design more "stable" MHPs.

26379368, 2024, 11, Downloaded from https://onlinelibrary.wiley.com/doi/10.1002/cey2.500, Wiley Online Library on [04/09/2026]. See the Terms and Conditions (https://onlinelibrary.wiley.com/terms-and-conditions) on Wiley Online Library for rules of use; OA articles are governed by the applicable Creative Commons License

Finally, the criterion of the time window of the stability test is still not clear and definite. Most of the experiments claimed that the MHP-based photocatalysts are stable in several recycle measurements, but the reaction time varies largely for different systems. For example, in some experiments, the reaction time is 4 h, while for others it could be 8 or 1 h. In this case, when performing the stability test, the total time shows a large scale from 4 to 40 h, which makes it not comparable in some cases. Besides, to meet the requirements of real-world practical applications, the criterion of the testing temperature should be included. For example, researchers can follow the same rules adopted in the perovskite solar cells, that is, under 85°C, to better evaluate the materials' stability. Therefore, before claiming "excellent" stability, the time window and the testing temperature should be considered.

ACKNOWLEDGMENTS

This work was financially supported by Hong Kong Research Grant Council (RGC) General Research Fund (GRF) (CityU 11305419, CityU 11306920, CityU 11308721, CityU 11316522) and SIRG 7020022.

CONFLICT OF INTEREST STATEMENT

The authors declare that there are no conflicts of interests.

ORCID

Chunhua Wang https://orcid.org/0000-0002-7763-6686
Yun Hau Ng https://orcid.org/0000-0001-9142-2126

REFERENCES

1. Wu X, Tan HL, Zhang C, et al. Recent advances in two-dimensional ultrathin Bi-based photocatalysts. *Prog Mater Sci*. 2023;133:101047.
2. Ding Y, Maitra S, Halder S, et al. Emerging semiconductors and metal-organic-compounds-related photocatalysts for sustainable hydrogen peroxide production. *Matter*. 2022;5(7):2119-2167.
3. Fujishima A, Honda K. Electrochemical photolysis of water at a semiconductor electrode. *Nature*. 1972;238(5358):37-38.
4. Pan S, Li J, Wen Z, et al. Halide perovskite materials for photo (electro) chemical applications: dimensionality, heterojunction, and performance. *Adv Energy Mater*. 2022;12(4):2004002.
5. Ding Y, Maitra S, Wang C, et al. Vacancy defect engineering in semiconductors for solar light-driven environmental remediation and sustainable energy production. *Interdiscip Mater*. 2022;1(2):213-255.
6. Rahaman M, Andrei V, Wright D, et al. Solar-driven liquid multicarbonfuel production using a standaloneperovskite–$BiVO_4$ artificial leaf. *Nat Energy*. 2023;8(6):629-638.
7. Teo SH, Ng CH, Ng YH, Islam A, Hayase S, Taufiq-Yap YH. Resolve deep-rooted challenges of halide perovskite for sustainable energy development and environmental remediation. *Nano Energy*. 2022;99(80):107401.
8. Andrei V, Ucoski GM, Pornrungroj C, et al. Floating perovskite-$BiVO_4$ devices for scalable solar fuel production. *Nature*. 2022;608(7923):518-522.
9. Bhattacharjee S, Rahaman M, Andrei V, et al. Photoelectrochemical CO_2-to-fuel conversion with simultaneous plastic reforming. *Nat Synth*. 2023;2(2):182-192.
10. Wang C, Zhang C, Wang S, et al. Low-temperature processed, efficient, and highly reproducible cesium-doped triple cation perovskite planar heterojunction solar cells. *Sol RRL*. 2018;2(2):1700209.
11. Rhee R, Kim TG, Jang GY, et al. Unassisted overall water splitting with a solar-to-hydrogen efficiency of over 10% by coupled lead halide perovskite photoelectrodes. *Carbon Energy*. 2023;5(1):e232.
12. Wang C, Ding Y, Liu B, Weng B, Hofkens J, Roeffaers MBJ. Crystal structure engineering of metal halide perovskites for photocatalytic organic synthesis. *Chem Commun*. 2023;59(21):3122-3125.
13. Wang J, Liu J, Du Z, Li Z. Recent advances in metal halide perovskite photocatalysts: properties, synthesis and applications. *J Energy Chem*. 2021;54:770-785.
14. Fu H. Colloidal metal halide perovskite nanocrystals: a promising juggernaut in photovoltaic applications. *J Mater Chem A*. 2019;7(24):14357-14379.
15. Wang J, Shi Y, Wang Y, Li Z. Rational design of metal halide perovskite nanocrystals for photocatalytic CO_2 reduction: recent advances, challenges, and prospects. *ACS Energy Lett*. 2022;7(6):2043-2059.
16. Park S, Chang WJ, Lee CW, Park S, Ahn HY, Nam KT. Photocatalytic hydrogen generation from hydriodic acid using methylammonium lead iodide in dynamic equilibrium with aqueous solution. *Nat Energy*. 2016;2(1):16185.
17. Chen S, Yin H, Liu P, Wang Y, Zhao H. Stabilization and performance enhancement strategies for halide perovskite photocatalysts. *Adv Mater*. 2023;35(6):2203836.
18. Fu Y. Stabilization of metastable halide perovskite lattices in the 2D limit. *Adv Mater*. 2022;34(9):2108556.
19. Kojima A, Teshima K, Shirai Y, Miyasaka T. Organometal halide perovskites as visible-light sensitizers for photovoltaic cells. *J Am Chem Soc*. 2009;131(17):6050-6051.
20. Liu XK, Xu W, Bai S, et al. Metal halide perovskites for light-emitting diodes. *Nat Mater*. 2021;20(1):10-21.
21. Tong S, Sun J, Wang C, et al. High-performance broadband perovskite photodetectors based on $CH_3NH_3PbI_3$/C8BTBT heterojunction. *Adv Electron Mater*. 2017;3(7):1700058.
22. Wu H, Ge Y, Niu G, Tang J. Metal halide perovskites for X-ray detection and imaging. *Matter*. 2021;4(1):144-163.
23. Li Z, Johnston A, Wei M, et al. Solvent-solute coordination engineering for efficient perovskite luminescent solar concentrators. *Joule*. 2020;4(3):631-643.
24. Wang C, Weng B, Liao Y, et al. Simultaneous photocatalytic H_2 generation and organic synthesis over crystalline–amorphous Pd nanocube decorated $Cs_3Bi_2Br_9$. *Chem Commun*. 2022;58(76):10691-10694.
25. Wang C, Weng B, Keshavarz M, et al. Photothermal Suzuki coupling over a metal halide perovskite/Pd nanocube

26379368, 2024, 11, Downloaded from https://onlinelibrary.wiley.com/doi/10.1002/cey2.500, Wiley Online Library on [04/09/2026]. See the Terms and Conditions (https://onlinelibrary.wiley.com/terms-and-conditions) on Wiley Online Library for rules of use; OA articles are governed by the applicable Creative Commons License

composite catalyst. *ACS Appl Mater Interfaces*. 2022;14(15):17185-17194.
26. Zhou J, Huang J. Photodetectors based on organic–inorganic hybrid lead halide perovskites. *Adv Sci*. 2018;5(1):1700256.
27. Wei Y, Wang W, Wang Z, et al. Recent progress of bismuth effect on all-inorganic lead-free metal halide derivatives: crystals structure, luminescence properties, and applications. *Adv Funct Mater*. 2023;33(2):2205829.
28. Steele JA, Prakasam V, Huang H, et al. Trojans that flip the black phase: impurity-driven stabilization and spontaneous strain suppression in γ-$CsPbI_3$ perovskite. *J Am Chem Soc*. 2021;143(28):10500-10508.
29. Duan J, Xu H, Sha WEI, et al. Inorganic perovskite solar cells: an emerging member of the photovoltaic community. *J Mater Chem A*. 2019;7(37):21036-21068.
30. Luo J, Zhang W, Yang H, et al. Halide perovskite composites for photocatalysis: a mini review. *EcoMat*. 2021;3(1):e12079.
31. Ding Y, Maitra S, Wang C, et al. Hydrophilic bi-functional B-doped g-C_3N_4 hierarchical architecture for excellent photocatalytic H_2O_2 production and photoelectrochemical water splitting. *J Energy Chem*. 2022;70:236-247.
32. Dey A, Ye J, De A, et al. State of the art and prospects for halide perovskite nanocrystals. *ACS Nano*. 2021;15(7):10775-10981.
33. Zhang J, Hodes G, Jin Z, Liu S. All-inorganic $CsPbX_3$ perovskite solar cells: progress and prospects. *Angew Chem Int Ed*. 2019;58(44):15596-15618.
34. Ravi VK, Markad GB, Nag A. Band edge energies and excitonic transition probabilities of colloidal $CsPbX_3$ (X= Cl, Br, I) perovskite nanocrystals. *ACS Energy Lett*. 2016;1(4):665-671.
35. Jin H, Debroye E, Keshavarz M, et al. It's a trap! On the nature of localised states and charge trapping in lead halide perovskites. *Mater Horiz*. 2020;7(2):397-410.
36. Tao S, Schmidt I, Brocks G, et al. Absolute energy level positions in tin-and lead-based halide perovskites. *Nat Commun*. 2019;10(1):2560.
37. Zhu W, Zhang Z, Chai W, et al. Band alignment engineering towards high efficiency carbon-based inorganic planar $CsPbIBr_2$ perovskite solar cells. *ChemSusChem*. 2019;12(10):2318-2325.
38. Tang Y, Tang S, Luo M, et al. All-inorganic lead-free metal halide perovskite quantum dots: progress and prospects. *Chem Commun*. 2021;57(61):7465-7479.
39. Zhao Z, Gu F, Rao H, et al. Metal halide perovskite materials for solar cells with long-term stability. *Adv Energy Mater*. 2019;9(3):1802671.
40. Aristidou N, Eames C, Sanchez-Molina I, et al. Fast oxygen diffusion and iodide defects mediate oxygen-induced degradation of perovskite solar cells. *Nat Commun*. 2017;8(1):15218.
41. Abdelmageed G, Jewell L, Hellier K, et al. Mechanisms for light induced degradation in $MAPbI_3$ perovskite thin films and solar cells. *Appl Phys Lett*. 2016;109(23):233905.
42. Ito S, Tanaka S, Manabe K, Nishino H. Effects of surface blocking layer of Sb_2S_3 on nanocrystalline TiO_2 for $CH_3NH_3PbI_3$ perovskite solar cells. *J Phys Chem C*. 2014;118(30):16995-17000.
43. Xiao M, Zhang Y, You J, et al. Addressing the stability challenge of metal halide perovskite based photocatalysts for solar fuel production. *J Phys Energy*. 2022;4(4):042005.
44. Ding Y, Wang C, Zheng R, et al. Three-dimensionally ordered macroporous materials for photo/electrocatalytic sustainable energy conversion, solar cell and energy storage. *EnergyChem*. 2022;4(4):100081.
45. Wang C, Zhang H, Lai F, et al. Engineering versatile Au-based catalysts for solar-to-fuel conversion. *J Energy Chem*. 2023;83(8):341-362.
46. Ding Y, Wang CH, Zhong JS, et al. Three-dimensionally ordered macroporous materials for pollutants abatement, environmental sensing and bacterial inactivation. *Sci China Chem*. 2023;66(7):1886-1904.
47. Peng Y, Zeng F, Cheng Y, et al. Fully Doctor-bladed efficient perovskite solar cells in ambient condition via composition engineering. *Org Electron*. 2020;83(10):105736.
48. Wang C, Yang J. Interface modification for organic and perovskite solar cells. *Sci China Mater*. 2016;59(9):743-756.
49. Ding R, Zhang X, Sun XW. Organometal trihalide perovskites with intriguing ferroelectric and piezoelectric properties. *Adv Funct Mater*. 2017;27(43):1702207.
50. Temerov F, Baghdadi Y, Rattner E, Eslava S. A review on halide perovskite-based photocatalysts: key factors and challenges. *ACS Appl Energy Mater*. 2022;5(12):14605-14637.
51. Buin A, Comin R, Xu J, Ip AH, Sargent EH. Halide-dependent electronic structure of organolead perovskite materials. *Chem Mater*. 2015;27(12):4405-4412.
52. Zhou Y, Zhao Y. Chemical stability and instability of inorganic halide perovskites. *Energy Environ Sci*. 2019;12(5):1495-1511.
53. Cheng S, Zhong H. What happens when halide perovskites meet with water? *J Phys Chem Lett*. 2022;13(10):2281-2290.
54. Leguy AMA, Hu Y, Campoy-Quiles M, et al. Reversible hydration of $CH_3NH_3PbI_3$ in films, single crystals, and solar cells. *Chem Mater*. 2015;27(9):3397-3407.
55. Murali B, Dey S, Abdelhady AL, et al. Surface restructuring of hybrid perovskite crystals. *ACS Energy Lett*. 2016;1(6):1119-1126.
56. Huang J, Tan S, Lund PD, Zhou H. Impact of H_2O on organic–inorganic hybrid perovskite solar cells. *Energy Environ Sci*. 2017;10(11):2284-2311.
57. You J, Yang Y, Hong Z, et al. Moisture assisted perovskite film growth for high performance solar cells. *Appl Phys Lett*. 2014;105(18):183902.
58. Wang C, Zhang C, Tong S, et al. Air-induced high-quality $CH_3NH_3PbI_3$ thin film for efficient planar heterojunction perovskite solar cells. *J Phys Chem C*. 2017;121(12):6575-6580.
59. Gong X, Li M, Shi XB, Ma H, Wang ZK, Liao LS. Controllable perovskite crystallization by water additive for high-performance solar cells. *Adv Funct Mater*. 2015;25(42):6671-6678.
60. Wang C, Huang H, Weng B, et al. Planar heterojunction boosts solar-driven photocatalytic performance and stability of halide perovskite solar photocatalyst cell. *Appl Catal B*. 2022;301:120760.
61. Christians JA, Miranda Herrera PA, Kamat PV. Transformation of the excited state and photovoltaic efficiency of $CH_3NH_3PbI_3$

26379368, 2024, 11, Downloaded from https://onlinelibrary.wiley.com/doi/10.1002/cey2.500, Wiley Online Library on [04/09/2026]. See the Terms and Conditions (https://onlinelibrary.wiley.com/terms-and-conditions) on Wiley Online Library for rules of use; OA articles are governed by the applicable Creative Commons License

perovskite upon controlled exposure to humidified air. *J Am Chem Soc*. 2015;137(4):1530-1538.
62. Yang J, Siempelkamp BD, Liu D, Kelly TL. Investigation of $CH_3NH_3PbI_3$ degradation rates and mechanisms in controlled humidity environments using in situ techniques. *ACS Nano*. 2015;9(2):1955-1963.
63. Mosconi E, Azpiroz JM, De Angelis F. Ab initio molecular dynamics simulations of methylammonium lead iodide perovskite degradation by water. *Chem Mater*. 2015;27(13):4885-4892.
64. Huang H, Pradhan B, Hofkens J, Roeffaers MBJ, Steele JA. Solar-driven metal halide perovskite photocatalysis: design, stability, and performance. *ACS Energy Lett*. 2020;5(4):1107-1123.
65. Zhang Y, Saidaminov MI, Dursun I, et al. Zero-dimensional Cs_4PbBr_6 perovskite nanocrystals. *J Phys Chem Lett*. 2017;8(5):961-965.
66. Du K, He L, Song S, et al. In situ embedding synthesis of highly stable $CsPbBr_3/CsPb_2Br_5$@PbBr(OH) nano/microspheres through water assisted strategy. *Adv Funct Mater*. 2021;31(36):2103275.
67. Liang T, Liu W, Liu X, Li Y, Wu W, Fan J. In situ phase-transition crystallization of all-inorganic water-resistant exciton-radiative heteroepitaxial $CsPbBr_3$–$CsPb_2Br_5$ Core–Shell perovskite nanocrystals. *Chem Mater*. 2021;33(13):4948-4959.
68. Di J, Li H, Su J, et al. Reveal the humidity effect on the phase pure $CsPbBr_3$ single crystals formation at room temperature and its application for ultrahigh sensitive X-ray detector. *Adv Sci*. 2022;9(2):2103482.
69. Akbali B, Topcu G, Guner T, Ozcan M, Demir MM, Sahin H. $CsPbBr_3$ perovskites: theoretical and experimental investigation on water-assisted transition from nanowire formation to degradation. *Phys Rev Mater*. 2018;2(3):034601.
70. Du K, Meng W, Wang X, Yan Y, Mitzi DB. Bandgap engineering of lead-free double perovskite $Cs_2AgBiBr_6$ through trivalent metal alloying. *Angew Chem Int Ed*. 2017;56(28):8158-8162.
71. Zhang S, Yuan Y, Gu J, et al. Surface defect-induced electronic structures of lead-free $Cs_2AgBiBr_6$ double-perovskite for efficiently solar-driven photocatalytic performance. *Appl Surf Sci*. 2023;609:155446.
72. Zhang C, Chen J, Kong L, et al. Core/shell metal halide perovskite nanocrystals for optoelectronic applications. *Adv Funct Mater*. 2021;31(19):2100438.
73. Chen Q, Ma Y, Wang L, Lan X, Shi J. Multifunctional melamine foam assisted lead halide perovskites for highly efficient and long-term photocatalytic CO_2 reduction under pure water. *Sol RRL*. 2021;5(5):2000755.
74. Romani L, Speltini A, Ambrosio F, et al. Water-stable $DMASnBr_3$ lead-free perovskite for effective solar-driven photocatalysis. *Angew Chem*. 2021;133(7):3655-3662.
75. Yin H, Chen J, Guan P, et al. Controlling photoluminescence and photocatalysis activities in lead-free $Cs_2Pt_xSn_{1-x}Cl_6$ perovskites via ion substitution. *Angew Chem Int Ed*. 2021;60(42):22693-22699.
76. Hong Z, Chong WK, Ng AYR, et al. Hydrophobic metal halide perovskites for visible-light photoredox C−C bond cleavage and dehydrogenation catalysis. *Angew Chem Int Ed*. 2019;58(11):3456-3460.
77. Wang H, Wang X, Chen R, et al. Promoting photocatalytic H_2 evolution on organic–inorganic hybrid perovskite nanocrystals by simultaneous dual-charge transportation modulation. *ACS Energy Lett*. 2018;4(1):40-47.
78. Wu Y, Wang P, Guan Z, et al. Enhancing the photocatalytic hydrogen evolution activity of mixed-halide perovskite $CH_3NH_3PbBr_{3-x}I_x$ achieved by bandgap funneling of charge carriers. *ACS Catal*. 2018;8(11):10349-10357.
79. Wu Y, Wang P, Zhu X, et al. Composite of $CH_3NH_3PbI_3$ with reduced graphene oxide as a highly efficient and stable visible-light photocatalyst for hydrogen evolution in aqueous HI solution. *Adv Mater*. 2018;30(7):1704342.
80. Wang X, Wang H, Zhang H, et al. Dynamic interaction between methylammonium lead iodide and TiO_2 nanocrystals leads to enhanced photocatalytic H_2 evolution from HI splitting. *ACS Energy Lett*. 2018;3(5):1159-1164.
81. Li R, Li X, Wu J, et al. Few-layer black phosphorus-on-$MAPbI_3$ for superb visible-light photocatalytic hydrogen evolution from HI splitting. *Appl Catal B*. 2019;259:118075.
82. Zhao Z, Wu J, Zheng YZ, Li N, Li X, Tao X. Ni_3C-decorated $MAPbI_3$ as visible-light photocatalyst for H_2 evolution from HI splitting. *ACS Catal*. 2019;9(9):8144-8152.
83. Cai C, Teng Y, Wu JH, et al. In situ photosynthesis of an $MAPbI_3$/CoP hybrid heterojunction for efficient photocatalytic hydrogen evolution. *Adv Funct Mater*. 2020;30(35):2001478.
84. Zhao X, Chen S, Yin H, et al. Perovskite microcrystals with intercalated monolayer MoS_2 nanosheets as advanced photocatalyst for solar-powered hydrogen generation. *Matter*. 2020;3(3):935-949.
85. Zhou P, Chen H, Chao Y, et al. Single-atom Pt-I_3 sites on all-inorganic Cs_2SnI_6 perovskite for efficient photocatalytic hydrogen production. *Nat Commun*. 2021;12(1):4412.
86. Tang Y, Mak CH, Liu R, et al. In situ formation of bismuth-based perovskite heterostructures for high-performance cocatalyst-free photocatalytic hydrogen evolution. *Adv Funct Mater*. 2020;30(52):2006919.
87. Guo Q, Zhang JD, Chen YJ, et al. Enhanced hydrogen evolution activity of $CsPbBr_3$ nanocrystals achieved by dimensionality change. *Chem Commun*. 2023;59(28):4189-4192.
88. Jiang Y, Li K, Wu X, et al. In situ synthesis of lead-free halide perovskite $Cs_2AgBiBr_6$ supported on nitrogen-doped carbon for efficient hydrogen evolution in aqueous HBr solution. *ACS Appl Mater Interfaces*. 2021;13(8):10037-10046.
89. Wang T, Yue D, Li X, Zhao Y. Lead-free double perovskite $Cs_2AgBiBr_6$/RGO composite for efficient visible light photocatalytic H_2 evolution. *Appl Catal B*. 2020;268:118399.
90. Zhang Y, Sun Z, Wang Z, Zang Y, Tao X. Efficient and long-term photocatalytic H_2 evolution stability enabled by $Cs_2AgBiBr_6/MoS_2$ in aqueous HBr solution. *Int J Hydrogen Energy*. 2022;47(14):8829-8840.
91. Guan Z, Wu Y, Wang P, et al. Perovskite photocatalyst $CsPbBr_{3-x}I_x$ with a bandgap funnel structure for H_2 evolution under visible light. *Appl Catal B*. 2019;245:522-527.

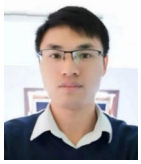
26379368, 2024, 11, Downloaded from https://onlinelibrary.wiley.com/doi/10.1002/cey2.500, Wiley Online Library on [04/09/2026]. See the Terms and Conditions (https://onlinelibrary.wiley.com/terms-and-conditions) on Wiley Online Library for rules of use; OA articles are governed by the applicable Creative Commons License

92. Xie K, Wei S, Alhadhrami A, et al. Synthesis of $CsPbBr_3$/$CsPb_2Br_5$@ silica yolk-shell composite microspheres: precisely controllable structure and improved catalytic activity for dye degradation. *Adv Compos Hybrid Mater*. 2022;5(2):1423-1432.
93. Gao J, Qian X, Wei Q, et al. Construction of core-shell cesium lead bromide-silica by precipitation coating method with applications in aqueous photocatalysis. *J Colloid Interface Sci*. 2022;623:974-984.
94. Li H, Zhang B, Zhang B, et al. Core-shell structured $CsPbBr_3$/Sn-TiO_2 nanocrystals for visible-light-driven photocatalyst in aqueous solution. *Appl Surf Sci*. 2022;599:153937.
95. Zhu J, Zhou L, Zhu Y, et al. Stable bismuth-doped lead halide perovskite core-shell nanocrystals by surface segregation effect. *Small*. 2022;18(3):2104399.
96. Kong ZC, Liao JF, Dong YJ, et al. Core@shell $CsPbBr_3$@zeolitic imidazolate framework nanocomposite for efficient photocatalytic CO_2 reduction. *ACS Energy Lett*. 2018;3(11):2656-2662.
97. Mu YF, Zhang W, Guo XX, Dong GX, Zhang M, Lu TB. Water-tolerant lead halide perovskite nanocrystals as efficient photocatalysts for visible-light-driven CO_2 reduction in pure water. *ChemSusChem*. 2019;12(21):4769-4774.
98. Wan S, Ou M, Zhong Q, Wang X. Perovskite-type $CsPbBr_3$ quantum dots/UiO-66 (NH_2) nanojunction as efficient visible-light-driven photocatalyst for CO_2 reduction. *Chem Eng J*. 2019;358:1287-1295.
99. Su K, Dong GX, Zhang W, Liu ZL, Zhang M, Lu TB. In situ coating $CsPbBr_3$ nanocrystals with graphdiyne to boost the activity and stability of photocatalytic CO_2 reduction. *ACS Appl Mater Interfaces*. 2020;12(45):50464-50471.
100. Wu LY, Mu YF, Guo XX, et al. Encapsulating perovskite quantum dots in iron-based metal–organic frameworks (MOFs) for efficient photocatalytic CO_2 reduction. *Angew Chem Int Ed*. 2019;58(28):9491-9495.
101. Xiao M, Hao M, Lyu M, et al. Surface ligands stabilized lead halide perovskite quantum dot photocatalyst for visible light-driven hydrogen generation. *Adv Funct Mater*. 2019;29(48):1905683.
102. Romani L, Bala A, Kumar V, et al. PEA_2SnBr_4: a water-stable lead-free two-dimensional perovskite and demonstration of its use as a co-catalyst in hydrogen photogeneration and organic-dye degradation. *J Mater Chem C*. 2020;8(27):9189-9194.
103. Ju D, Zheng X, Liu J, et al. Reversible band gap narrowing of Sn-based hybrid perovskite single crystal with excellent phase stability. *Angew Chem Int Ed*. 2018;57(45):14868-14872.
104. García T, García-Aboal R, Albero J, Atienzar P, García H. Vapor-phase photocatalytic overall water splitting using hybrid methylammonium copper and lead perovskites. *Nanomaterials*. 2020;10(5):960.
105. Da P, Cha M, Sun L, Wu Y, Wang ZS, Zheng G. High-performance perovskite photoanode enabled by Ni passivation and catalysis. *Nano Lett*. 2015;15(5):3452-3457.
106. Wang C, Yang S, Chen X, Wen T, Yang HG. Surface-functionalized perovskite films for stable photoelectrochemical water splitting. *J Mater Chem A*. 2017;5(3):910-913.
107. Hoang MT, Pham ND, Han JH, Gardner JM, Oh I. Integrated photoelectrolysis of water implemented on organic metal halide perovskite photoelectrode. *ACS Appl Mater Interfaces*. 2016;8(19):11904-11909.
108. Nam S, Mai CTK, Oh I. Ultrastable photoelectrodes for solar water splitting based on organic metal halide perovskite fabricated by lift-off process. *ACS Appl Mater Interfaces*. 2018;10(17):14659-14664.
109. Tao R, Sun Z, Li F, Fang W, Xu L. Achieving organic metal halide perovskite into a conventional photoelectrode: outstanding stability in aqueous solution and high-efficient photoelectrochemical water splitting. *ACS Appl Energy Mater*. 2019;2(3):1969-1976.
110. Hamdan M, Chandiran AK. Cs_2PtI_6 halide perovskite is stable to air, moisture, and extreme pH: application to photoelectrochemical solar water oxidation. *Angew Chem*. 2020;132(37):16167-16172.
111. Poli I, Hintermair U, Regue M, et al. Graphite-protected $CsPbBr_3$ perovskite photoanodes functionalised with water oxidation catalyst for oxygen evolution in water. *Nat Commun*. 2019;10(1):2097.
112. Crespo-Quesada M, Pazos-Outón LM, Warnan J, Kuehnel MF, Friend RH, Reisner E. Metal-encapsulated organolead halide perovskite photocathode for solar-driven hydrogen evolution in water. *Nat Commun*. 2016;7(1):12555.
113. Gao LF, Luo WJ, Yao YF, Zou ZG. An all-inorganic lead halide perovskite-based photocathode for stable water reduction. *Chem Commun*. 2018;54(81):11459-11462.
114. Zhang H, Yang Z, Yu W, et al. A sandwich-like organolead halide perovskite photocathode for efficient and durable photoelectrochemical hydrogen evolution in water. *Adv Energy Mater*. 2018;8(22):1800795.
115. Ahmad S, Sadhanala A, Hoye RLZ, et al. Triple-cation-based perovskite photocathodes with AZO protective layer for hydrogen production applications. *ACS Appl Mater Interfaces*. 2019;11(26):23198-23206.
116. Kim JH, Seo S, Lee JH, et al. Efficient and stable perovskite-based photocathode for photoelectrochemical hydrogen production. *Adv Funct Mater*. 2021;31(17):2008277.
117. Wang M, Li Y, Cui X, et al. High-performance and stable perovskite-based photoanode encapsulated by blanket-cover method. *ACS Appl Energy Mater*. 2021;4(8):7526-7534.
118. Chen J, Yin J, Zheng X, et al. Compositionally screened eutectic catalytic coatings on halide perovskite photocathodes for photoassisted selective CO_2 reduction. *ACS Energy Lett*. 2019;4(6):1279-1286.
119. Rahaman M, Andrei V, Pornrungroj C, Wright D, Baumberg JJ, Reisner E. Selective CO production from aqueous CO_2 using a $Cu_{96}In_4$ catalyst and its integration into a bias-free solar perovskite–$BiVO_4$ tandem device. *Energy Environ Sci*. 2020;13(10):3536-3543.
120. Zhang H, Chen Y, Wang H, et al. Carbon encapsulation of organic–inorganic hybrid perovskite toward efficient and stable photo-electrochemical carbon dioxide reduction. *Adv Energy Mater*. 2020;10(44):2002105.
121. Andrei V, Reuillard B, Reisner E. Bias-free solar syngas production by integrating a molecular cobalt catalyst with perovskite-$BiVO_4$ tandems. *Nat Mater*. 2020;19(2):189-194.

26379368, 2024, 11, Downloaded from https://onlinelibrary.wiley.com/doi/10.1002/cey2.500, Wiley Online Library on [04/09/2026]. See the Terms and Conditions (https://onlinelibrary.wiley.com/terms-and-conditions) on Wiley Online Library for rules of use; OA articles are governed by the applicable Creative Commons License

122. Li ZJ, Hofman E, Li J, et al. Photoelectrochemically active and environmentally stable $CsPbBr_3/TiO_2$ core/shell nanocrystals. *Adv Funct Mater*. 2018;28(1):1704288.
123. Tang X, Yang J, Li S, et al. Single halide perovskite/semiconductor core/shell quantum dots with ultrastability and nonblinking properties. *Adv Sci*. 2019;6(18):1900412.
124. Zhu Y, Liu Y, Ai Q, et al. In situ synthesis of lead-free halide perovskite–COF nanocomposites as photocatalysts for photoinduced polymerization in both organic and aqueous phases. *ACS Mater Lett*. 2022;4(3):464-471.
125. Zhang Z, Liu L, Huang H, et al. Encapsulation of $CsPbBr_3$ perovskite quantum dots into PPy conducting polymer: exceptional water stability and enhanced charge transport property. *Appl Surf Sci*. 2020;526:146735.
126. Wang H, Wang X, Zhang H, Ma W, Wang L, Zong X. Organic−inorganic hybrid perovskites: game-changing candidates for solar fuel production. *Nano Energy*. 2020;71:104647.
127. Shyamal S, Pradhan N. Halide perovskite nanocrystal photocatalysts for CO_2 reduction: successes and challenges. *J Phys Chem Lett*. 2020;11(16):6921-6934.
128. Liu GN, Zhao RY, Xu B, et al. Design, synthesis, and photocatalytic application of moisture-stable hybrid lead-free perovskite. *ACS Appl Mater Interfaces*. 2020;12(49):54694-54702.
129. Latini A, Quaranta S, Menchini F, et al. A novel water-resistant and thermally stable black lead halide perovskite, phenyl viologen lead iodide $C_{22}H_{18}N_2(PbI_3)_2$. *Dalton Trans*. 2020;49(8):2616-2627.
130. Aamir M, Shah ZH, Sher M, et al. Enhanced photocatalytic activity of water stable hydroxyl ammonium lead halide perovskites. *Mater Sci Semicond Process*. 2017;63:6-11.
131. Spanopoulos I, Hadar I, Ke W, et al. Water-stable 1D hybrid tin(II) iodide emits broad light with 36% photoluminescence quantum efficiency. *J Am Chem Soc*. 2020;142(19):9028-9038.

AUTHOR BIOGRAPHIES



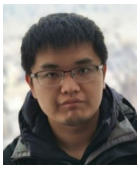
Chunhua Wang received his PhD degree from the Division of Molecular Imaging and Photonics, KU Leuven, Belgium, in 2022 studying solar-driven catalytic applications of metal halide perovskites, under the supervision of Prof. Johan Hofkens and Prof. Maarten Roeffaers. He is currently a postdoctoral research fellow in the group of Prof. Yun Hau Ng, at the Laboratory of Catalysis for Alternative & Renewable Energy, City University of Hong Kong. His current research focuses on synthesizing nanomaterials especially metal halide perovskites, investigating their fundamental properties, and applications in photocatalytic solar-to-chemical energy conservation.



Yang Ding is currently a distinguished associate professor at the College of Materials and Environmental Engineering, Hangzhou Dianzi University, China. He received his PhD degree from the Laboratory of Inorganic Materials Chemistry (CMI), University of Namur, Belgium, in 2022 under the supervision of Prof. Bao-lian Su. His research fields include fluorescent material synthesis, porous photocatalyst design, optoelectronic device construction and sustainable energy production.



Yannan Wang is currently a PhD researcher in the Department of Materials Engineering, KU Leuven, Belgium. She majors in sustainable metallurgy, under the supervision of Prof. Bart Blanpain and Dr. Muxing Guo. She will defence in January 2024 and then join the Hong Kong University of Science and Technology for Mars concrete research. Her current research focuses on psychical chemistry, reaction thermodynamics and kinetics.



Zhirun Xie is currently a postdoctoral research fellow in the group of Prof. Yun Hau Ng, at the Laboratory of Catalysis for Alternative & Renewable Energy, City University of Hong Kong. He received his PhD degree in Chemical Engineering from the University of New South Wales (UNSW) in 2020 under the supervision of Prof. Yun Hau Ng and Prof. Jason Scott. His research interest focuses on the design of efficient photo(electro) catalysts for solar energy conversion and utilization.



Zhiyuan Zeng is an assistant professor in Department of Materials Science and Engineering, City University of Hong Kong. He obtained his B.E. and M.E. from Central South University, Zhejiang University, in 2006 and 2008, respectively. He completed his PhD at Nanyang Technological University, Singapore (2013). He started his postdoctoral training at Lawrence Berkeley National Laboratory (2013–2017), followed by Senior Engineer at Applied Materials Inc. (2017–2019, Silicon Valley); he joined CityU in 2019. His research interests include lithium intercalation & exfoliation method for 2D TMDs, in situ liquid phase TEM, energy and environmental research.

26379368, 2024, 11, Downloaded from https://onlinelibrary.wiley.com/doi/10.1002/cey2.500, Wiley Online Library on [04/09/2026]. See the Terms and Conditions (https://onlinelibrary.wiley.com/terms-and-conditions) on Wiley Online Library for rules of use; OA articles are governed by the applicable Creative Commons License



Xin Li is a professor at the South China Agricultural University. He received his BS and PhD degrees in chemical engineering from Zhengzhou University in 2002 and the South China University of Technology in 2007, respectively. Then, he joined South China Agricultural University as a faculty staff member and became a professor in 2017. During 2012 and 2019, he worked as a visiting scholar at the Electrochemistry Center, the University of Texas at Austin, and the Department of Chemistry, the University of Utah, respectively. His research interests include photocatalysis, photoelectrochemistry, adsorption, biomass engineering and related materials, and devices development.



Yun Hau Ng is a professor at the School of Energy and Environment, and the director of Low-Carbon and Climate Impact Research Centre (LCCIC) at City University of Hong Kong. He received his PhD degree (Chemistry) from Osaka University in 2009. After brief attachment at the University of Notre Dame, he moved to Australia and became a lecturer at the University of New South Wales (UNSW) in 2014. He joined CityU in 2018. His research is focused on the development of novel photoactive semiconductors (particles and thin films) for sunlight energy conversion, including hydrogen generation from water and conversion of carbon dioxide to solar fuels. He received a few recognitions in photocatalysis research, including *Honda-Fujishima* Prize (2013), *Distinguished Lectureship Award* from the Chemical Society of Japan (2018), *APEC Science Prize for Innovation, Research and Education (ASPIRE)* in Chile (2019), and *Kataoka Lectureship Award* from the Japanese Photochemistry Association (2021).

How to cite this article: Wang C, Ding Y, Wang Y, et al. Metal halide perovskites for solar-to-chemical energy conversion in aqueous media. *Carbon Energy*. 2024;6:e500. doi:10.1002/cey2.500

26379368, 2024, 11, Downloaded from https://onlinelibrary.wiley.com/doi/10.1002/cey2.500, Wiley Online Library on [04/09/2026]. See the Terms and Conditions (https://onlinelibrary.wiley.com/terms-and-conditions) on Wiley Online Library for rules of use; OA articles are governed by the applicable Creative Commons License